

# Two-photon-assisted polymerization and reduction : emerging formulations and applications

Lay, Chee Leng; Koh, Charlynn Sher Lin; Lee, Yih Hong; Phan-Quang, Gia Chuong; Sim, Howard Yi Fan; Leong, Shi Xuan; Han, Xuemei; Phang, In Yee; Ling, Xing Yi

2020

Lay, C. L., Koh, C. S. L., Lee, Y. H., Phan-Quang, G. C., Sim, H. Y. F., Leong, S. X., ... Ling, X. Y. (2020). Two-photon-assisted polymerization and reduction : emerging formulations and applications. *ACS Applied Materials & Interfaces*, 12(9), 10061-10079.  
doi:10.1021/acsami.9b20911

<https://hdl.handle.net/10356/143426>

<https://doi.org/10.1021/acsami.9b20911>

---

This document is the Accepted Manuscript version of a Published Work that appeared in final form in *ACS Applied Materials & Interfaces*, copyright © American Chemical Society after peer review and technical editing by the publisher. To access the final edited and published work see <https://doi.org/10.1021/acsami.9b20911>

*Downloaded on 20 Mar 2024 17:39:11 SGT*

# Two-photon-assisted Polymerization and Reduction: Emerging Formulations and Applications

Chee Leng Lay,<sup>†‡</sup> Charlynn Sher Lin Koh,<sup>†</sup> Yih Hong Lee,<sup>†</sup> Gia Chuong Phan-Quang,<sup>†</sup> Howard Yi Fan Sim,<sup>†</sup> Shi Xuan Leong,<sup>†</sup> Xuemei Han,<sup>†</sup> In Yee Phang,<sup>\*‡</sup> and Xing Yi Ling<sup>\*†</sup>

<sup>†</sup> Division of Chemistry and Biological Chemistry, School of Physical and Mathematical Sciences, Nanyang Technological University, 21 Nanyang Link, Singapore 637371.

<sup>‡</sup> Institute of Materials Research and Engineering, Agency for Science, Technology and Research (A\*STAR), 2 Fusionopolis Way, Innovis, #08-03, Singapore 138634.

**KEYWORDS:** Two-photon lithography, two-photon polymerization, two-photon reduction, direct metal writing, 3D nanofabrication, hydrogel/organogel photoresists, metal salt-based photoresists

Two-photon lithography (TPL) is an emerging approach to fabricate complex multifunctional micro-/nanostructures. This is because of it can easily develop various 2D and 3D structures on various surfaces, and there has been a rapidly expanding pool of processable photoresists to create different materials. However, challenges in developing two-photon processable photoresists currently impedes progress in TPL. In this review, we critically discuss the importance of photoresist formulation in TPL. We begin by evaluating the available commercial photoresists to design micro-/nanostructures for promising applications in anti-counterfeiting, superomniphobicity, and micro-machines with movable parts. Next, we discuss emerging hydrogel/organogel photoresists, focusing on customizing photoresist formulation to fabricate reconfigurable structures which can respond to changes in local pH, solvent, and temperature. We also review the development of metal salt-based photoresists for direct metal writing, whereby various formulations have been developed to enable applications in online sensing, catalysis, and electronics. Finally, we provide a critical outlook and highlight various outstanding challenges in formulating processable photoresists for TPL.

## 1. INTRODUCTION

Advances in lithography-based fabrication techniques have enabled the printing of targeted micro-/nanostructures with intricate architecture. These structures have found applications across diverse fields such as biomedical research,<sup>1</sup> optics,<sup>2-3</sup> surface coatings,<sup>4-5</sup> and anti-counterfeiting.<sup>6-7</sup> For example, bespoke tissue engineering scaffolds can be three dimensionally printed to match a patient's anatomical geometries for tissue regeneration and reconstructive surgery.<sup>8-9</sup> Two-photon lithography (TPL) stands out among various lithographic approaches to fabricate customized two- and three-dimensional (2D, 3D) structures and surfaces. This is because TPL is a direct writing and maskless stereolithographic technique, whereby femtosecond laser pulses are raster scanned through a photoresist in a layer-by-layer fashion and micro-/nanostructures are created in a single fabrication step.

TPL achieves a sub-diffraction-limited structural resolution of  $\sim 70$  nm despite being a light-based technique,<sup>10</sup> and this capability allows TPL to generate structures possessing nanoscale features. This superior resolution arises from the underlying third-order nonlinear optical processes based on the two-photon absorption of TPL to achieve photoexcitation. The equation  $E \propto (I)^2 \propto (1/d)^4$  rationalizes the non-linear dependence of the excitation rate ( $E$ ) of photoactive molecules present in the photoresist on laser irradiation intensity ( $I$ ) and distance ( $d$ ) from the laser focal plane.<sup>2, 11</sup> Consequently, photoexcitation and hence photopolymerization/photoreduction only occurs within regions of highest laser irradiation intensity along the laser excitation path. Experimentally, these regions correspond to a tightly confined laser focal volume, which have typical values of  $\sim 2.2 \times 10^{-4} \mu\text{m}^3$ . There is minimal uncontrolled photochemical reaction occurring beyond the laser focal spot. This nonlinear optical process also allows deeper irradiation

penetration (penetration depth  $\geq 300 \text{ }\mu\text{m}$ ) into the photoresist for precise photopolymerization/photoreduction in the three Cartesian planes, thereby enabling the fabrication of complex details down to the nanoscale. For example, large area anti-counterfeiting patterns<sup>12-13</sup> and atomic force microscopy (AFM) tips<sup>14</sup> have been fabricated in a single step using TPL, which are otherwise unachievable by other stereolithographic techniques.<sup>10</sup>

TPL as a direct writing technique offers significantly higher versatility in structural design and geometry control as compared to other stereolithography techniques such as one-photon lithography (OPL) and electron beam lithography (EBL).<sup>15</sup> TPL offers a host of easily customizable fabrication and processing parameters to users in structural fabrication, including laser exposure time, laser power, laser scanning path, photoresist choice and formulation, as well as pre- and post-fabrication processing steps. Together with its sub-diffraction-limited resolution, high-resolution 3D micro-/nanostructures of various material composition can be easily fabricated. In contrast, OPL cannot fabricate hierarchical or elaborate 3D microstructures due to its inferior resolution in the z-direction.<sup>16</sup> This limitation arises from the intrinsic linear single-photon absorption process driving OPL, which leads to uncontrolled excitation of photoactive precursors along the entire irradiation pathway.<sup>16</sup> On the other hand, making well-aligned and well-defined 3D microstructures using EBL is a tedious multi-step process involving repetitive rounds of photoresist film deposition, positional alignment, electron beam writing, and structural development.<sup>17</sup> This process is repetitive because the photoresist film thickness is typically limited to the nanometer range to allow uniform exposure to the electron beam, but this nanosized thickness hinders the formation of 3D structures in a single electron beam exposure.<sup>18</sup> Moreover, the requirement of high vacuum conditions for EBL-based fabrication precludes using liquid-based photoresists to form micro/nanostructures, and this limitation further restricts the types of materials

available for structural fabrication. These comparisons clearly highlight the advantages of TPL over OPL and EBL in fabricating 3D complex structures in the sub-micrometer to micrometer scale.

In TPL, photoresists play a central role in realizing tailorable 2D/3D structures, with their properties and/or formulations directly impacting the ability to create well-defined features. Photoresists broadly refer to the light-sensitive resin used in TPL and a typical photoresist formulation comprises photoinitiators, monomers, crosslinkers, and solvents to dissolve the individual components for liquid-based photoresists. During TPL, photoinitiators first undergo localized two-photon absorption from the high-energy laser irradiation within the confocal volume. Subsequently, a charge transfer process occurs between the photoinitiators and monomers to kick-start a free radical-based polymerization reaction between the monomer units in the confocal volume. During both the raster scanning and layer-by-layer writing processes, polymerization continues within overlapping regions of the confocal volume, leading to the formation of 3D extended polymer networks. The presence of crosslinkers with multiple unsaturated bonds further contributes towards the construction of 3D structural network via the formation of covalent bonds between various polymer chains and the crosslinkers. By controlling the polymerization extent and bonding strength between polymer chains, photoresist formulation thus directly impacts the structural integrity and mechanical properties of the resultant polymeric 2D/3D structures. Generally, ideal photoresists for TPL should possess the following five characteristics:<sup>3, 19</sup> (1) photoinitiators should have sufficient two-photon absorptivity near the two-photon excitation wavelength to trigger photopolymerization; (2) photoresists should be rapidly curable within the confined laser focal spot to avoid overheating; (3) photoresists should be optically transparent in the same spectral window as the incident irradiation to prevent linear

absorption, irradiation blockage and generation of excess heat; (4) photoresists should be optimally viscous to avoid structural deformation during TPL; (5) photoresists should be able to produce mechanically stable structures that can withstand the development and solvent washing process post-TPL. Photoresists exhibiting these five characteristics will enable the fabrication of large-area structures with unique architecture and consistent properties.

A wide variety of photoresists is available for TPL, and the choice of suitable photoresist(s) ultimately depends on the desired functionalities of the final product and its target applications. In this review, we categorize photoresists into two groups based on the intrinsic photochemical processes occurring during TPL, namely photoresists that undergo two-photon polymerization (TPP) or two-photon reduction (TPR). TPP photoresists comprise photoinitiators, polymerizable monomers and crosslinkers in their formulations. Examples of TPP photoresists are commercial acrylate-based, epoxy-based, phenol-formaldehyde-based, organic-inorganic hybrid photoresists, as well as emerging hydrogel photoresists made of proteins or sulfonic acids. In particular, hydrogel photoresists are quickly gaining attention because the use of such photoresists in TPL has led to micro-/nanostructures exhibiting dynamic properties which are otherwise not possible using commercial photoresists, including stimuli-responsiveness,<sup>20-21</sup> biomimetic self-actuation,<sup>22-23</sup> and shape-shifting capabilities.<sup>24-25</sup> Collectively, these TPP-fabricated functional micro-/nanostructures have found applications in cell proliferation studies,<sup>1</sup> micromachining,<sup>26-27</sup> surface-enhanced Raman scattering (SERS) sensing,<sup>28</sup> anti-counterfeiting<sup>6, 21</sup> as well as stimuli-responsive nanoactuation<sup>23</sup> (Tables 1 and 2). On the other hand, TPR photoresists comprise metal salts, reducing agents and capping agents. TPR involves the photothermal-induced direct formation of metallic micro-/nanostructures via the reduction of metal salts, and is also known as direct metal writing (DMW).<sup>29-30</sup> During DMW, the high intensity of the tightly confined laser

spot generates tremendous heat, which reduces metal salts into metal atoms and produces nuclei (seeds) for subsequent growth into nanoparticles.<sup>30</sup> These nanoparticles further form clusters along the raster-scanning laser paths to become 2D/3D metallic structures.<sup>29</sup> Mild reducing agents such as ethylene glycol<sup>31</sup> or trisodium citrate<sup>32</sup> are also added to the formulation to accelerate the photothermal reduction process. Capping agents adsorb onto the nanoparticles surfaces during DMW to stabilize the metallic particles by generating repulsive electrostatic forces or steric hindrance at the surface, thus preventing random uncontrollable agglomeration.<sup>30</sup> Using metal salt-containing photoresists enables a direct one-step fabrication of metallic nanostructures without the need for multiple deposition and etching steps. These metallic nanostructures can be used as electronic circuit components,<sup>33-34</sup> sensors, catalysts<sup>35</sup> and metamaterials on substrates<sup>36</sup> (Table 3).

Indeed, the emergence of TPL as a versatile fabrication technique to create a plethora of micro-/nanostructures with wide-ranging applications is evident from the various review articles published to date. These reviews cover a comprehensive range of topics including TPL mechanisms and system setup,<sup>2-3</sup> types of photoinitiators,<sup>1, 3</sup> and fabrication of microstructures using commercial photoresists.<sup>37</sup> However, there is currently a lack of in-depth discussion on how photoresist formulations impact subsequent micro-/nanostructure fabrication and applications, despite growing research in tailoring new stimuli-responsive hydrogel- and metal salt-based photoresists to fabricate metallic structures. It is crucial to focus on photoresists and their formulations because they play critical roles in fabricating structurally robust micro-/nanostructures via TPL. An overview of the latest developments can drive progress in structural fabrication and develop new applications more effectively.

Herein, we review the development of TPL photoresists, focusing on how photoresists types and formulations influence the properties and applications of the fabricated micro-/nanostructures. We

divide our discussion into three sections according to the types of photoresists, namely commercial photoresists, stimuli-responsive hydrogel/organogel photoresists, and metal salt-containing photoresists (Figure 1). We begin with emerging applications of static micro-/nanostructures fabricated using well-established commercial photoresists, including anti-counterfeiting, surface wettability control and microengineering. Next, we discuss recent progress in formulating various types of hydrogel/organogel photoresists based on different stimuli (pH, solvent, ion and temperature) for the fabrication of various dynamic structures, including self-actuating microvalves, microlens and microsensors. We will highlight the factors influencing the fabrication of these microstructures and their responsiveness towards stimuli. In the last section, we will delve into the use of metal salt-based photoresists to directly fabricate metal nanoparticle arrays via TPR and discuss their applications in sensing, catalysis, electronic circuits and 2D/3D metamaterials. Finally, we conclude our discussion with a critical outlook of several grand challenges in this research field. By providing an overview of the current trends in this field, we hope that these insights can stimulate the development of new photoresists and applications across a broad range of disciplines including chemistry, optics, plasmonics, microfluidics, surface science/engineering and biomimetics.

## **2. CONVENTIONAL PHOTORESISTS AND THEIR USE FOR UNCONVENTIONAL APPLICATIONS: ANTI-COUNTERFEITING, ANTI-WETTING AND MICROENGINEERING**

Acrylate-based (e.g. IP® series) and bisphenol A novolac epoxy-based (e.g. SU-8 series) photoresists are two of the most commonly used commercial TPL photoresists. These photoresists

meet the five requirements discussed above: they are viscous, optically transparent at the excitation wavelength, and possess photoinitiators with sufficient two-photon absorptivity to enable rapid formation of mechanically and chemically stable structures. Furthermore, they are ready-to-use, require minimal pre-fabrication preparation, and often have well-established fabrication protocols. These attributes significantly simplify the fabrication process and facilitate the construction of high-resolution well-defined micro-/nanostructures with established applications as cell scaffolds,<sup>1</sup> photonic crystals,<sup>38</sup> and prototypes.<sup>3, 37</sup> Without having to refine photoresist formulation for specific structural fabrication, commercial photoresists enable researchers to focus on designing unique and customized structures for new applications. In this section, we highlight the use of commercial photoresists for developing functional structures with emerging applications as security labels, superomniphobic surfaces, and microrobots.

**2.1. Commercial Photoresists for Security Labels.** The ability of TPL to fabricate large-area uniform structures presents a unique opportunity to fabricate optical security labels to combat counterfeiting. An optical security label typically encodes molecular information within an array of structures. Such information is not accessible by examining the physical features of the labels. Successful decoding of the covert information requires knowledge of the label design and advanced spectroscopic imaging techniques, such as confocal fluorescence imaging and/or surface-enhanced Raman scattering (SERS) hyperspectral imaging. Consequently, security labels demand the fabricated micro-/nanostructures to exhibit high structural fidelity across large areas, as well as the ability to encode multiple layers of covert molecular information within an array of structures without signal crosstalk.

TPL enables judicious control over the process of security label fabrication, whereby it can spatially and selectively embed various layers of covert molecular information within the TPL-written structures. Typical optical security labels comprise arrays of nanopillars and/or wires, which can be routinely generated through conventional TPL approach (Figure 2). Fluorescence information can be encoded within the structures by doping commercial photoresists with fluorophores prior to the fabrication process. Following TPL fabrication, further coating the array with plasmonic-active metallic films or nanoparticles renders the platform SERS-active. This metallization step also allows vibrational fingerprints of the fluorophores embedded within the fabricated structures to be readout via SERS. In addition, the surface of the metallic film or nanoparticles can be further functionalized with other SERS-active molecules to increase information encoding density (Figure 2B).<sup>12</sup> Every fluorescence emission peak and unique molecular vibrational mode serve as individual layers of encoded information in these optical security labels. Importantly, these arrays show up as ordinary structures under optical and electron microscopy characterizations. Subsequent spectroscopic imaging reveals various layers of covert molecular patterns, such as Taiji motifs,<sup>39</sup> Merlion images,<sup>12</sup> and machine-readable quick-response (QR) code (Figure 2).<sup>6</sup> A combination of fluorescent and SERS readouts enables five layers of encryption within a single 2D platform of nanopillars. Up to seven layers of information can be encoded within an array by tuning the polarization-dependent SERS readout intensity (Figure 2C (i)).<sup>40</sup> However, the limited surface area of the plasmonic structures in the x-y plane restricts the addition of multiple probe molecules for further security enhancement. Hence, there is an increasing need to exploit the z-dimension of the security labels and extend the information density within an array in 3D.

Extending anti-counterfeiting platforms from 2D to 3D increases the encoded data density in the same area, thus increasing the difficulty of deciphering the encoded molecular information and deterring imitation. Multiple layers of covert 2D images can be selectively stacked at different focal planes along the z-axis of an array of 3D microstructures, generating various z-axis-dependent signal readouts. For instance, by encoding an array of candlestick microstructures with various heights using a single type of molecule, up to three layers of graphical patterns can be selectively revealed without crosstalk by extracting SERS images at specific z values (Figure 3A).<sup>13</sup> Similarly, selectively loading more than two types of quantum dots in the voids of a 3D crossed grid also reveals highly z-dependent numerical patterns via fluorescence imaging (Figure 3B).<sup>7, 41</sup> Furthermore, TPL enables these 3D microstructures to be fabricated on both rigid substrates (e.g. glass or silicon wafer) and flexible polymer films (e.g. polyethylene terephthalate) without compromising structural resolution and stability, further widening their potential usage to curved product surfaces and banknotes.<sup>13</sup> In contrast, conventional mask-based stereolithography techniques requires expensive photomasks and limits the ease of structural fabrication.<sup>15</sup>

To stay ahead of counterfeiters, the patterns of the security labels should be constantly renewed. For instance, hybrid security labels can be generated by combining miniaturized conventional covert features such as holograms or watermarks with fluorescence- or SERS-based micro-/nanostructures. Additional verification channels can also be created by generating multi-stack features comprising of various materials and molecular encoding.

**2.2 Commercial Photoresists for Superomniphobic (SPOP) Surfaces.** With its ability to fabricate large-area microstructures with nanoscale features, TPL enables the fabrication of superomniphobic (SPOP) surfaces, which can repel both water and oils effectively. Doubly re-

entrant structures are central in realizing SPOP surfaces; these are microscale columnar structures with nanoscale overhanging and flat-top mushroom-shaped suspending features (Figure 4).<sup>4-5, 42</sup> Such overhanging features change the meniscus shape of liquids to cause an upward supporting force, countering liquid wetting and maintaining liquid droplet sphericity on surfaces (Figure 4A(i)).<sup>42</sup> The use of sufficiently viscous photoresists in TPL enables fabrication of doubly re-entrant structures for SPOP surfaces, where liquid turbulence induced by system vibration during fabrication are minimized and thus retaining the overhanging/suspending features.<sup>4</sup> In contrast, conventional subtractive approaches and nanoimprint lithography require multiple processing steps to fabricate similar structures, including physical/chemical etching, laser ablation and alignment.<sup>42</sup> These multi-step approaches are time-consuming, require careful control over experimental parameters, and use expensive toxic/corrosive chemicals. In addition, conventional subtractive approaches can only fabricate the structures on rigid silicon substrates, which significantly limits their applications as SPOP and super-repellent coatings on curved surfaces (e.g. inner lining of bottles and convex mirrors at roads with sharp turnings). Thus far, acrylate-based photoresist has been successfully used to fabricate doubly re-entrant microstructures with designs such as double-layered doubly re-entrant microstructures (Figure 4A)<sup>4</sup> and slippery lubricant infused doubly re-entrant microstructures (Figure 4B).<sup>5</sup> These designs allow numerous solvents to exhibit static contact angle  $> 150^\circ$  when they are in contact with the surface, including water (surface tension = 72 mN/m) and n-perfluorooctane (surface tension = 14 mN/m).<sup>43</sup>

A major limitation of current TPL-fabricated SPOP surfaces arises from the use of extra additives such as lubricants to repel liquids.<sup>5</sup> These lubricants are normally low surface-tension fluorinated oils, which are volatile and thus require frequent re-coating on the SPOP platform to maintain liquid repellency (Figure 4B(ii)). This re-coating also poses risks of sample

contamination.<sup>5</sup> Hence, further improvements on structural designs and surface chemistry are essential to achieve SPOP without using these additives. Furthermore, it is critical for the doubly re-entrant microstructures to withstand repetitive impact, compressive and shear forces when they are used for self-cleaning and anti-smudge applications. While there is no report on the structural stability of these structures, we envision the need to reinforce the mechanical robustness of these structures because such structures typically exhibit high aspect ratios ( $> 30\text{-}\mu\text{m}$  tall structures) and are unlikely to be sufficiently structurally robust to withstand the wear and tear during application.

**2.3 Commercial Photoresists for Micromachine.** One of the greatest fabrication process of TPL lies in its ability to generate movable microstructures which can be lifted-off from substrates post-fabrication and then suspended in liquids. These structures are termed micromachines, and they are designed to perform tasks such as environmental remediation, therapeutics, cargo transport and diagnostics in narrow and confined spaces.<sup>26-27, 44</sup> These functions are typically inaccessible to their larger counterparts. Fabricating such micromachines using conventional subtractive techniques and NIL remain challenging, because these techniques cannot fabricate moving parts such as chain- or joint-like features as well as structures with helical or void components. On the other hand, TPL can generate helical structures and dangling parts of a substrate-adhered microdevice with ease, such as microturbine<sup>45</sup> and force-sensing microgripper.<sup>46</sup> Using TPL, highly mobile helical micromachines and compound micromachines (comprising a set of microhelical plunger and cylindrical capsule) have been designed and fabricated via either acrylate- or epoxy-based photoresists (Figure 5A, 5B).<sup>26, 44</sup> Typically, the movements of these micromachines can be either self-propelled by incorporating hydrogen peroxide-sensitive metals on the microstructures' surfaces (Figure 5C)<sup>27</sup> or manipulated by external magnetic field when the

surfaces of the micromachines are coated with magnetic nanoparticles.<sup>26, 44</sup> This achievement is crucial in paving the way towards realizing actual applications of these complex micromachines.

The three emerging applications of TPL discussed heretofore establishes its capability to achieve precise micro-/nanoscale structural fabrication. However, the current success of TPL is built upon the predominant use of commercial acrylate- or epoxy-based photoresists (Table 1), resulting in static structures which are not responsive to external stimuli. This bottleneck hinders the expansion of TPL towards fabricating dynamic and responsive structures which can achieve on-demand and on-site actuation. On this note, TPL nanofabrication of dynamic microstructures using hydrogel photoresists containing stimuli-responsive components are gaining extensive attention.

### **3. CUSTOMIZED HYDROGEL/ORGANOGE L PHOTORESISTS FOR STIMULI-RESPONSIVE STRUCTURES IN TPL**

Stimuli-responsive microstructures can be readily fabricated using TPL by leveraging on its ability to achieve localized microscale control over the polymerization process.<sup>20-25, 47</sup> These structures are typically 3D polymeric network structures with high solvent contents, such as hydrogels and organogels, and they are formed through radical polymerization during TPL. Common hydrogel structures include protein-based<sup>24-25, 47</sup> and olefinic polymers<sup>22-23</sup> while organogel structures include photocurable polydimethylsiloxane (PDMS) and acrylates.<sup>20-21</sup> By using monomers and/or oligomers with different functional groups, these microstructures can respond to stimuli such as pH,<sup>24-25, 47</sup> solvent,<sup>20</sup> moisture,<sup>21</sup> ions<sup>22</sup> and temperature.<sup>23</sup> In contrast, ultraviolet lithography (UVL) and EBL pose significant limitations in the fabrication of complex self-actuating microstructures. Current microscopic UVL can only fabricate millimeter-scale responsive

structures. Microscale resolution remains a challenge particularly for hydrogel structures due to the difficulty in controlling crosslinking density accurately among smaller structures.<sup>48-49</sup> EBL requires high vacuum operating conditions and thus renders it incompatible with the use of evaporative aqueous-based hydrogel photoresists. Consequently, TPL emerges as an ideal technique to fabricate programmable stimuli-responsive and self-actuated micro-/nanostructures. These structures are highly appealing for the delivery and controlled-release of therapeutics, *in-situ* sensing and diagnostics, responsive photonic displays, as well as flow control in microfluidic devices.<sup>18, 34-40</sup>

Various fabrication parameters can be modulated during TPL to control the extent of polymerization and crosslinking density in the resultant micro-/nanostructures, and by extension the responsiveness of these structures towards stimuli. In general, lower laser power, shorter dwell time, or larger z-layer distance results in lower crosslinking density, in turn generating less compact structures, which exhibit greater responsiveness (Figure 6).<sup>24-25, 47</sup> The responsiveness of a microstructure is typically quantified using its swelling ratio, which measures the changes in area/volume arising from stimulus relative to its original state. Notably, TPL can fabricate shape-shifting systems with different responsiveness in the same structure by creating regions of different polymerization/crosslinking degree within a single structure, achieved through a simple programming of writing parameters. In addition, the high spatiotemporal resolution of TPL enables the construction of sophisticated 3D high-aspect-ratio ( $> 5$ ) shape-changing microstructures.<sup>23, 50</sup>

In the absence of commercially available photoresists to create smart microstructures, the challenge is to formulate photoresists that can fabricate dynamic microstructures with good structural integrity and exhibit fast responsiveness. As with all other photoresists, the customized stimuli-responsive hydrogel/organogel photoresists must meet the as-mentioned requirements for

ideal photoresist to be two-photon processable. Because the microstructures' responsiveness also depends on its intrinsic properties (e.g. the amount/type of responsive functional groups in structure), stimuli-responsive photoresists for TPL must be carefully customized with appropriate functional group(s) containing monomers, crosslinkers, photoinitiators and/or viscosity enhancing agents. In the following section, we discuss the types of hydrogels/organogels based on the stimulus (pH, solvent, ion and temperature) and illustrate how the combination of TPL and stimuli-responsive photoresists achieves 2D/3D smart materials such as microvalves, microlens and microsensors.

**3.1 pH-responsive Shape-Change Structures and Applications.** pH-responsive gels can expand or shrink in response to changes in surrounding pH, and are typically protein-based (e.g. bovine serum albumin (BSA)) because they contain multiple pH-responsive functional groups such as carboxylic and amino acids.<sup>24-25, 47</sup> At isoelectric pH, the proteins are uncharged and are hydrophobic. This results in increased protein intermolecular interactions and repulsion of water from the polymer network which causes the protein gel to shrink. On the other hand, the protein chains become ionized due to deprotonation/protonation of its carboxylic/amino acids at basic/acidic pH. Repulsion of like charges on the proteins promote interactions with water molecules, thereby causing the protein gel to swell.

BSA-based photoresists have been successfully formulated to fabricate uniform pH-responsive microstructures. Typical BSA photoresists contain rose bengal (RB) as photoinitiator, BSA as monomer, crosslinker and viscosity regulating agent, dimethyl sulfoxide and phosphate buffer saline as solvents.<sup>24-25, 50-51</sup> Optimized RB concentration should be greater than 4 mM to generate sufficient free radicals upon laser irradiation to initiate photopolymerization.<sup>50</sup> BSA concentration

should be above 290 g/L so that there are sufficient polymerizable and crosslinkable functional groups to enable structural formation. However, at this BSA concentration, the photoresist is not viscous enough and the fabricated microstructures may be structurally distorted.<sup>50</sup> The viscosity of BSA photoresists can be increased by evaporating the solvents in an oven,<sup>51</sup> or introducing viscosity enhancing polymers such as polyvinylpyrrolidone (PVP).<sup>50</sup> To achieve sufficient viscosity without additional processing step, BSA concentration should be above 460 g/L so that the minimum viscosity reaches 37 cP.<sup>50</sup> By using optimally formulated BSA photoresists, the uniform swelling of microstructures such as BSA microsieves for active selection of particles or cells in a microfluidic device has been demonstrated (Figure 6A).<sup>47</sup>

More recently, TPL also enables the fabrication of single-component BSA microstructures, which can undergo anisotropic and programmable shape-change. Using TPL, anisotropic responsiveness across a single BSA structure can be achieved by generating various regions of different polymerization/crosslinking degree within the same structure (Figure 6B).<sup>24</sup> For instance, by adopting a “bimetallic strip” design strategy, two combined BSA strips with different crosslinking density bends upon pH change due to the difference in swelling degree in each strip. Such dynamic bending in the protein strips has been employed to create a BSA-based Venus fly trap. (Figures 6C- 6F).<sup>24</sup> Additionally, by patterning microstructures with alternating low and highly crosslinked segments, reversible geometrical circle-to-polygon and polygon-to-circle shape shifting can be readily achieved through pH changes (Figure 6G, 6H).<sup>25</sup> Collective geometrical shape-change of these microstructures also leads to transformative 2D patterned arrays with dynamic variation in array pore sizes.<sup>25</sup>

While BSA-based pH-responsive systems are highly promising, there are some limitations, which need to be addressed. BSA is a well-known biological adhesive.<sup>52</sup> This property may render

BSA microstructures with high surface stickiness: once two BSA structures are in contact during swelling, it is deduced that the contacted surfaces may not separate even after shrinking. And, this sticking may cause structural damage and device failure. Moreover, prolonged pH-reversible change cycles may cause fatigue in BSA microstructures which reduces their pH-responsiveness. Besides BSA, there are few reports on the development of other pH-responsive photoresists suitable for TPL. Consequently, the current challenge is to find new substitutions of BSA that can achieve better and more sustainable pH-responsive performance.

**3.2 Solvent- and Ion-responsive Photoresists and Applications.** Solvent-responsive hydrogels/organogels contain responsive chemical groups that expand/shrink when in contact with different solvents/humidity, and are usually fabricated from olefinic materials. The swelling extent correlates with the amount of solvents absorbed into the hydrogels/organogels, which is governed by the affinity between chemical groups of hydrogels/organogels and solvent molecules. For example, photoresists containing vinyl-terminated polydimethylsiloxanes (PDMS) are used to fabricate solvent-responsive hyperboloid micro-lens (Figure 7A).<sup>20</sup> The nanoscale resolution and precise movement control of TPL allow the fabrication of highly smooth hyperboloid microlens (surface roughness  $\approx 7\text{nm}$ ) with low surface defects. The presence of organic solvents causes the PDMS hyperbolic structure to swell, and the extent of swelling depends on the solubility of the organic solvent in PDMS. Such swelling changes the curvature of the hyperbolic structure, thus enabling a systematic tuning of the micro-lens' focal length from  $112 - 185\ \mu\text{m}$  as the solvent changes from water to n-hexane.<sup>20</sup>

On the other hand, water-responsive poly(ethylene glycol) diacrylate (PEG-DA) hydrogel structures have demonstrated utility as humidity sensors and information encryption.<sup>21</sup> PEG-DA

structures are fabricated from aqueous-based photoresists comprising methylene blue as photoinitiators and PEG-DA as the building blocks. The hydrophilic hydroxyl groups on the PEG-DA backbone allow the formation of hydrogen bonds with water molecules, and the adsorption of water causes PEG-DA structures to swell. PEG-DA hydrogel slabs having ‘stomata’ structures can be used to qualitatively estimate the relative humidity of the environment, by determining the changes in aperture size of the stomata. In information encryption, binary codes are fabricated by strategically positioning responsive PEG-DA micropillars amongst micropillars made of inert methacrylate materials.<sup>21</sup> Subsequent introduction of water vapor enables the PEG-DA micropillars to selectively swell and reveal the covert binary codes corresponding to a pre-designed set of alphabetical and numerical information.

Photoresists of PDMS and PEG-DA have relatively high viscosity, thus enabling them to be directly used for structural fabrication without additional processing step or additive for viscosity improvement. However, the response rates of these materials towards solvents are 10-fold slower than BSA hydrogels, taking a minimum of 4 s.<sup>20-21</sup> Therefore, the challenge for these gels is to formulate photoresists to improve subsequent responsiveness of the fabricated structures.

To enhance responsiveness, suitable ionic monomers/oligomers can be incorporated to the photoresist formulation. For example, ionic monomers such as 2-acrylamido-2-methylpropane sulfonic acid sodium (AMPS) can be polymerized with PEG-DA or acrylamide (AAm) matrix to confer ion-responsive properties to the resultant microstructures.<sup>22</sup> In water, the poly(AAm-AMPS) chains swell and exhibit extended conformation due to the electrostatic repulsive force exerted by sulfonic acid groups. Introducing salts in the solution screens this charge repulsion, resulting in polymer chain coiling and shrinking of the poly(AAm-AMPS) chains. By fabricating “bimetallic” ion-responsive microcantilevers with AAm-AMPS photoresist, large bending angles

of  $\sim 33^\circ$  can be achieved within one second upon immersing the microcantilevers in water and sodium chloride solution (Figure 7B).<sup>22</sup> While the response time has improved, such microcantilevers distort and display inconsistent responses towards salt solutions. This inconsistency arises from the low viscosity of the aqueous-based AAm-AMPS photoresist, which generates mechanical vibration-induced turbulence during TPL fabrication. This example clearly demonstrates the difficulty in formulating aqueous-based photoresists to achieve the best viscosities and stimuli-responsiveness.

**3.3 Temperature-responsive Photoresists and Applications.** Thermo-responsive gels typically employ poly(*N*-isopropylacrylamide) (PNIPAAm) as material of choice. PNIPAAm polymer chains have a reversible lowest critical solution temperature (LCST) phase transition between 32 to 33 °C.<sup>23</sup> As the local temperature increases to LCST, the initially water-soluble PNIPAAm polymer chain undergoes a thermodynamically-driven coil-to-globule transition by expelling adsorbed water. This phase transition causes phase separation and volume shrinkage. An optimized heat-responsive photoresist has been reported, comprising *N*-isopropylacrylamide (NIPAAm) as monomers, *N,N'*-methylenebisacrylamide as crosslinkers, and lithium phenyl(2,4,6-trimethylbenzoyl)phosphinate as photoinitiator.<sup>23</sup> High viscosity ethylene glycol is used as solvent in place of water, to prevent structural distortion arising from mechanical vibration during TPL. Well-defined PNIPAAm microcantilevers with “bimetallic” configuration and consistent properties are fabricated with this photoresists formulation,<sup>23</sup> exhibiting better structural integrity than those fabricated from water-based photoresists.<sup>22</sup> Notably, the thermal-responsive motion of the PNIPAAm structures can be reversibly actuated either by changing the bulk water temperature

or by locally illuminating the desired microstructure with a focused laser to induce photo-to-thermal conversion.

The development of various stimuli-responsive microstructures via TPL is evidently an emerging field, which gives rise to a plethora of opportunities previously not thought possible. However, there are still issues that limit the progress in this area, including inconsistent photoresist formulation, low-viscosity of aqueous photoresists, and lack of suitable aqueous photoinitiators. Majority of the stimuli-responsive photoresists are not yet commercially available because solvent evaporation over time gives rise to inconsistent concentration of active components. Water and volatile organic liquids such as methanol and ethanol are common solvents in responsive photoresists; even optimal storage/usage conditions do not prevent their inevitable evaporation which leads to fluctuations in the photoresist formulation. Another photoresist-related issue is the low viscosity of aqueous photoresists: most of the powdered or particulate precursors have limited solubility in water and/or have low molecular weight (e.g. vinyl monomers) which does not contribute to increasing the viscosity of the photoresists.<sup>22-23</sup> As a result, complex structures such as suspending or helical features cannot be fabricated because they will topple due to gravity. Structural distortion and inconsistent responsiveness are also commonly observed among simpler structures.<sup>22, 50</sup> While some approaches have been proposed in the earlier discussion e.g. solvent evaporation and addition of high molecular weight-polymers, it is challenging to achieve similar batch-to-batch photoresist consistency through simple solvent evaporation. Moreover, the addition of inert polymers may affect the responsiveness of the written microstructures. With regards to photoinitiators, the most commonly used photoinitiators in aqueous-based photoresists are rose bengal and commercial  $\alpha$ -hydroxyketone based photoinitiators because they are the only water-soluble photoinitiators. However, these photoinitiators suffer from low two-photon absorption

cross-sections. It is therefore imperative to develop water-soluble photoinitiators with high two-photon absorption and charge transfer efficiency to improve the fabrication process.<sup>53-54</sup> Possible candidates include benzylidene cyclopentanone and cyclohexanone dyes.<sup>53-54</sup> Successfully addressing these concerns can potentially enable the fabrication of smart microstructures capable of more sophisticated motions to mimic bio-organisms found in nature, such as reversible self-folding origami<sup>55-56</sup> or retractable flaps for propulsion.<sup>57</sup>

#### **4. METAL SALTS-BASED PHOTORESISTS FOR METALLIC STRUCTURES**

The high peak power of a femtosecond pulsed laser ( $10^3$ - $10^6$  W) allows direct photothermal-induced reduction of metallic salts into functional metallic 2D/3D micro-/nanostructures with nanoscale precision. This one-step fabrication process is more commonly known as direct metal writing (DMW). Metallic structures are conventionally fabricated via a series of nanoimprint and etching processes, but these processes often involve multiple expensive and time-consuming fabrication steps. Although inkjet printing of metal colloids offers high printing resolution with well-defined structures on designated areas,<sup>58</sup> this method still heavily relies on the time-consuming *ex-situ* synthesis of metallic particles. Consequently, the goal of simplifying the fabrication process drives the exploration of DMW to create metallic micro-/nanostructures, particularly for applications in compact micro-/nanoelectronic systems, photonic devices, plasmonic sensors and metamaterials/metasurfaces.

There are two categories of photoresists for DMW: (1) aqueous-based metal salt solutions for 2D structures (Figure 8A),<sup>31, 35, 59</sup> and (2) a combination of metal salt solutions and polymer supportive matrices for 3D structures (Figure 8B).<sup>36, 60</sup> Both aqueous and polymer-matrix based DMW photoresists are composed of metal salts, particle-size controlling capping agents and

photosensitizers.<sup>29-30</sup> The metal salt is the most important component in two-photon reduction (TPR). Suitable metal salts for TPR should possess positive standard reduction potentials; the most commonly used metal salts are silver- (Ag, standard reduction potential = 0.7996 V) and gold- (Au, standard reduction potential = 1.498 V) based metal salts.<sup>61</sup> Capping agents control the particle sizes by minimizing unwanted growth of metallic nanoparticles, and common capping agents include PVP,<sup>31, 62</sup> poly(4-styrenesulfonic acid),<sup>63</sup> n-decanoyl sarcosine sodium<sup>64</sup> and hexadecyltrimethyl ammonium bromide (CTAB).<sup>65</sup> Photosensitizers boost the photosensitivity of the TPR process by generating more electrons/radicals in the photoresists, in turn enhancing the reduction rates of metal ions. Consequently, laser dwell time can be reduced, leading to improved resolution of the fabricated metallic structures.<sup>66</sup> Adding photosensitizers such as (2-hydroxy-4'-(2-hydroxyethoxy)-2-methylpropiophenone (HHMP),<sup>64</sup> (2,4,6-trimethylbenzoyl)-phosphine oxide (TPO)<sup>65</sup> and Coumarin 440<sup>67</sup> has been shown to improve DMW efficiency and structural resolution by at least 30%. Mild reducing agents such as ethylene glycol<sup>31</sup> or trisodium citrate<sup>32</sup> can also be introduced to expedite the photothermal reduction processes. In type 2 photoresists, polymer matrices such as gelatin,<sup>60</sup> acrylic<sup>36</sup> and SU-8<sup>68</sup> facilitate the fabrication of 3D metallic structures. The polymer matrices are infused with metallic ions and contain large amounts of polar –C-O-C, –C=O, –COOH or –NH<sub>2</sub> functionalities, serving both as capping agents and as physical supports to stabilize the as-synthesized 3D metallic structures.<sup>60</sup> In the following section, we will focus on the recent progress of DMW to fabricate emerging functional microstructures for electronic applications, SERS sensing and detection, microfluidics and 3D metamaterials (Table 3).

**4.1 DMW Metallic Structures for Electronic Applications.** The flexibility of TPL in writing metallic micro-/nanostructures enables DMW to be employed for the fabrication of integrated electronic circuits. The general DMW process involves only two procedures - two-photon irradiation and sample washing. In contrast, conventional micromachining methods such as EBL, etching, and metal deposition require multiple processing steps that are time-consuming and costly. The first attempt of DMW created electronic circuits with resolution between 2 to 12  $\mu\text{m}$ , using photoresists containing only aqueous solution of silver nitrate ( $\text{AgNO}_3$ ) or tetrachloroauric acid ( $\text{HAuCl}_4$ ) for fabrication of Ag and Au structures, respectively.<sup>59</sup> In subsequent attempts, a 10-fold reduction in the linewidths of the fabricated structures is achieved by introducing mild reducing agents and photoinitiators to the metal salt photoresists.<sup>67, 69</sup> These additions allow control over the reduction rate of the metal ions and hence the final particle sizes and surface roughness.

DMW can also fabricate metallic circuits on various surfaces, ranging from hard substrates like glass<sup>67-68</sup> and silicon wafers<sup>36</sup> to flexible polymeric substrates<sup>70</sup> for flexible electronic devices. However, the main challenge is to reduce the electrical resistivity of the fabricated Ag or Au micropatterns before they can be used in electronic circuits (Figure 8A).<sup>33-34</sup> While the resistivity of these 1D/2D metallic structures range from  $10^{-6} \Omega\text{m}$  to  $10^{-7} \Omega\text{m}$  and is similar to those of metallic structures fabricated via EBL,<sup>71</sup> these resistivities are 3 to 20 times larger than their bulk metals commonly used in circuits ( $\sim 10^{-8} \Omega\text{m}$ ).<sup>34, 62, 68, 72</sup> This higher resistivity arises from disconnected metallic lines, presence of residual stabilizing agents on the nanoparticles, and oxidation of nanoparticles.<sup>59</sup> While post-fabrication treatments such as annealing and electrodeless plating are used to change the particulate morphology and reduce surface roughness, they do not lead to significant improvement in electronic property. Hence, there is a need to improve

photoresist formulations to enable better control over particle size, density and particle distribution to achieve reproducible analysis and better conductivities.<sup>29</sup>

**4.2 DMW Metallic Structures for Online Microfluidic Sensing and Detection.** The high penetration depth of TPL enables it to directly write metallic structures within enclosed microfluidic channels for SERS detection. In particular, online microfluidic analysis with SERS detection (“online SERS”) is an emerging detection technique in the bio/chemical analytical field. The microfluidic setup allows rapid and high throughput sensing capacity with low sample volume ( $\leq 100 \mu\text{L}$ ),<sup>73</sup> while SERS detection affords ultrasensitive signals with specific molecular fingerprints. Conventional online SERS platforms utilize solutions containing metal colloidal particles but often suffer from random particle aggregation with time, and inconsistent hotspot density within laser spot, which causes irregular signal intensity. DMW overcomes these limitations by affixing the written metallic patterns on the inner sidewall of the channel, providing a static and reproducible hotspot ‘bed’ that allow accurate laser alignment. The hotspot density within the laser excitation volume thus remains constant throughout the fluidic analysis, which in turns gives consistent signal intensity.

To facilitate infusion of photoresists into microfluidic channels, aqueous-based metal salt solutions are normally used. For instance, 2D patterns made of Au nanoparticles are photoreduced from polyvinylpyrrolidone (PVP)-containing ethylene glycol/water solution of  $\text{HAuCl}_4$ .<sup>31</sup> The resultant microfluidic channel is employed for versatile online SERS sensing of gaseous ethanol and acetone as they sequentially diffuse through the microfluidic channel (Figure 8B).<sup>31</sup> The microfluidic channel is therefore useful for detection of chemical vapors which have no specific affinity to metal surfaces and have very weak Raman scattering cross-sections. Notably, the SERS

hotspot density of the Au-nanoparticle arrays can be increased by increasing concentration of PVP up to 30 wt% in the photoresist, which boosts the SERS enhancement factor of the Au-patterned arrays from  $5.6 \times 10^4$  to  $2.8 \times 10^5$ .<sup>31</sup> PVP can adsorb onto the Au nanoparticles and reduce the size of Au nanoparticles from 65 nm to 27 nm, thus effectively increasing the Au nanoparticle and hence SERS hotspot density from 172 to 965 particles/ $\mu\text{m}^2$ .<sup>31</sup> In addition, various 2D/3D Ag microstructures of different geometries (pillars, stars and cubes) are also successfully fabricated within a microfluidic channel for SERS sensing via DMW. The photoresist contains trifluoroacetic acid silver salt ( $\text{CF}_3\text{COOAg}$ ) as metallic precursor, poly(4-styrenesulfonic acid) as capping agent, and ruthenium (II) tris(bipyridine) as photoinitiator.<sup>63</sup> Notably, the analytical enhancement factor of these metallic patterns reaches  $10^8$ , comparable to SERS platforms fabricated via other particle assembly methods.<sup>65</sup> This highlights that DMW is an attractive alternative to *in-situ* produce high quality nanoparticles for development of automatic and high-throughput microfluidic devices with ultrasensitive SERS sensing.

**4.3 DMW 2D Metallic Structures for Catalysis.** The combination of a single-step DMW with small photoresist volumes ( $\leq 1 \text{ mL}$ ) provides an eco-friendly way to generate metallic micro/nanostructures for catalysis as compared to large-volume solvent-based chemical reactions. Metal-based materials are widely accepted as efficient and reliable catalysts in accelerating chemical reactions, thus driving the development of nanosized metallic catalysts using DMW. DMW can fabricate uniformly dispersed catalytically active sites at specific locations within 3D microchambers/microfluidic channels, facilitating the design of multi-functional microfluidic channels. In contrast, other methods such as sputtering, atomic layer deposition and simple dusting only produce non-uniform thin films within microfluidic channels. Additionally, DMW can

localize the position of the nanocatalysts within microfluidic channels to enable online reaction monitoring and screening via spectroscopic techniques such as SERS. Such *in-situ* kinetic investigation is challenging to perform with other platforms.

For instance, arrays of 2D round Ag microflowers are fabricated within a microfluidic channel via DMW, using an aqueous-based photoresist containing  $\text{AgNO}_3$ , trisodium citrate, and ammonia.<sup>32</sup> Ammonia stabilizes the silver ions by forming  $\text{Ag}(\text{NH}_3)^{2+}$  so that the Ag ions will not undergo uncontrollable chemical reduction caused by trisodium citrate during DMW. Notably, on-chip catalytic reduction of 4-nitrophenol shows that the Ag microflowers have high catalytic activity (100% chemical conversion in 7 minutes) and strong SERS enhancement (enhancement factor  $\approx 10^8$ ).<sup>32</sup> In addition, platinum (Pt) based 2D microstructures are generated through DMW using ammonium tetrachloroplatinate (II) salt and ammonium trisoxalatoferrate (III) trihydrate as a photosensitizer.<sup>35</sup> The decomposition of hydrogen peroxide over these Pt microstructures releases oxygen gas which can induce fluid flow in specific directions within the microchambers and channels (Figure 8C(ii)).<sup>35</sup> Notably, DMW also showcases its precision in multi material patterning (Figure 8C(i)). However, the use of trisoxalatoferrate (III) trihydrate requires the formation of an iron (II) reducing agent upon laser irradiation before reducing Pt, thus requiring longer laser exposure and slowing down the DMW process. Despite the potential advantages of DMW catalysts over conventional catalysts, there are limited works on creating metallic microreactors within microfluidic devices via TPL. This could be due to the limited types of transition metals which can undergo photothermal reduction rapidly and are catalytically active. Moreover, most metallic structures are restricted to 2D configurations which limit catalytic efficiencies and reaction rates. Arrays with 3D network-like or close-packed helical metallic structures are more desirable to increase surface area for enhanced catalysis.

**4.4 DMW 2D Metallic Structures for Split-Ring Resonators.** The excellent spatial resolution of TPL enables DMW to generate C-shaped or U-shaped Au split-ring resonators (SRRs) with very small slit gap distances (Figure 8D).<sup>72</sup> SRRs are metamaterial structures for generating media with wavelength-dependent tunable refractive indices. A SRR consists of a pair of concentric non-magnetic metallic rings with slits etched on opposite side of the rings. To achieve magnetic susceptibility with terahertz resonance frequencies, slit gap distance must be smaller than the targeted frequency and possess high array periodicity.<sup>64</sup> EBL and DMW are normally employed to fabricate SRRs with controllable dimensions and well-defined alignment. While EBL has high resolution of  $\geq 2$  nm, DMW surpasses EBL in fabricating SRRs in terms of fabrication speed because DMW effectively reduces the tedious procedures necessitated by EBL into two simple steps: writing and rinsing.<sup>74-75</sup> Therefore, DMW has high potential to fabricate non-conventional electronic devices such as SRRs which can have applications in superlens, cloaking, radio astronomy and satellite communications. The key challenge is the need to prevent ohmic losses of the split-ring resonator due to the scattering from surface imperfections and from grain boundaries because the DMW-fabricated structures are formed from metallic nanoparticles.

To tackle this problem, ionic liquid ((2-hydroxyethyl)trimethylammonium 5-aminopentanoic) can be added into the photoresist as capping agent to reduce surface roughness by reducing particle size to 5 nm and improving the line resolution ( $\approx 228$  nm) of the fabricated metallic micro/nanostructures.<sup>72</sup> The resultant 2D arrays of U-shaped Au SRRs possess uniform distribution of electric field across the substrates at the resonant frequency. Furthermore, arrays of these U-shaped Au SRRs only selectively generate electric resonance of approximately 63 THz when interacting with x-polarized wave.<sup>72</sup> In addition, the concentration of metal ions must be

optimized for different photoreduction formulation because excess metal ions may cause structure roughening and result in scattering loss. On the other hand, insufficient metal ions may induce discontinuity and decrease in the conductivity. With the optimized conditions, arrays of C-shaped SRRs with homogeneous properties are fabricated via DMW (Figure 8D).<sup>64, 76</sup> Therefore, we have showcased that 2D metallic structures have several potential emerging applications. However, their performance (e.g. sensing and reduction) is constrained by their limited functional surface area to interact with targeted molecules. Moreover, their plasmonic property and electrical conductivity may also be interfered by the substrate support.

**4.5 DMW 3D Metallic Microstructures.** Moving beyond 2D metallic structures, DMW also has the capability to print 3D metallic micro-/nanostructures with controlled geometries. These 3D metallic structures are useful for applications in microelectronics, 3D integrated circuits (ICs), micro-/nano-electromechanical systems, metamaterials, and sensors.<sup>77-78</sup> DMW is proficient in the fabrication of 3D metallic structures of higher complexity because the 3D structures can be fabricated within polymer/aqueous solutions, polymer gel matrices or organic-inorganic frameworks via a direct and one-step photoreduction of metal salts.<sup>62, 76</sup> To date, the most commonly used approaches to fabricate 3D metallic micro-/nanostructures are the subtractive EBL,<sup>79</sup> localized pulsed electrodeposition,<sup>80</sup> template-assisted electro-/electroless plating<sup>38, 81-82</sup> and focused ion beam (FIB) milling.<sup>80</sup> Although FIB is capable of producing arbitrary shape microstructures via ultra-precision milling and grinding, it involves time-consuming sample preparation and is prone to damaging the surface of the manufactured samples.<sup>80</sup> EBL and localized pulsed electrodeposition are also too slow (nanometer per second) for practical applications.<sup>79-80</sup> While template-assisted electro-/electroless plating enable rapid fabrication of

freestanding metallic structures with well-defined size and shape,<sup>38, 81-82</sup> such methods also require additional steps for fabrication of the template and its removal at the end of the process.<sup>38, 81</sup>

The first 3D metallic microstructure is an Ag gate microstructure with the smallest linewidth of 2  $\mu\text{m}$ ; it is freestanding on a glass substrate without support.<sup>59</sup> The DMW process uses  $\text{AgNO}_3$  aqueous-based solution without photosensitizer. However, it remains highly challenging to fabricate large-area freestanding 3D metallic structures with complex designs via DMW using aqueous-based photoresists. During DMW of a metallic structure on a substrate, there is a difference in metal reduction rate between the glass-solution boundary and the solution, with much higher reduction speeds occurring at the glass-solution boundary. To maintain consistent reduction, the laser power must be constantly adjusted during fabrication and this may affect structural properties of the 3D metallic microstructures. Moreover, as with hydrogel photoresists, there are fluidic turbulences in low-viscosity water-based metallic photoresists. Formation of 3D metallic structures is impossible if particle diffusion and convection is faster than particle nucleation and growth, wherein newly formed metallic nanoparticles drift away from instead of adhering to the already written structures. To deal with these issues, PVP/ $\text{AgNO}_3$  film is first thermally dried before DMW to create 3D pyramidal microstructures.<sup>62</sup> However, heating PVP/ $\text{AgNO}_3$  salt solution may cause premature heat-induced reduction of Ag ions, as well as inhomogeneous drying of the PVP/ $\text{AgNO}_3$  film. These issues may impact DMW efficiency and uniformity in properties of the written structures.<sup>62</sup>

The first complex, freestanding 3D metallic framework is achieved by using a photoresist combining containing nickel-based (Ni) organometallic compound with nickel acrylate and pentaerythritol triacrylate (Figure 9).<sup>36</sup> In contrast to metal salts which have < 10 wt% solubility in polymer photoresists, organometallic precursors improve the concentration of metal ions in

polymer matrices to almost 20 wt%. This thus permits the written 3D structures to retain their predesigned full metallic structures after pyrolysis and annealing. The complex 3D Ni structures have excellent mechanical properties, which create various opportunities in the engineering of photonic and optoelectronic devices and is a breakthrough for the emerging trend of high-performance metamaterial engineering.

Overall, the main advantage of DMW over conventional methods lies in its fabrication simplicity yet without compromising on structural resolution. However, we recognize that DMW is unable to achieve continuous crystalline metal structures. Currently, the resulting lithography-written metallic structures are still particle-based which comprise of nanoparticles or nanoscale clusters even after annealing. This issue imposes poor electrical conductivity, high surface inhomogeneity and forms structures that are prone to collapsing.<sup>11</sup> As a result, metal-salt based photoresists are still premature for practical 3D additive nanofabrication. Moving forward, further research on optimizing metal writing conditions in terms of photoresist compositions is imperative to achieve a smooth and continuous metal surface for practical applications. In addition, we expect the inclusion of multiple metals on a substrate<sup>35</sup> or within a hydrogel/polymer matrix<sup>83</sup> to further extend potential of the DMW technique on creating multifunctional metallic structures.

## **5. CONCLUSION AND PERSPECTIVE OF TPL**

In this review, we have elaborated on the latest developments in TPL, focusing on the importance of photoresist formulation in fabricating various micro-/nanostructures. We have also emphasized on how TPL paves the way for trending applications in anti-counterfeiting, super-repellent surfaces, microfluidics, microelectronics and smart microstructures/devices. TPL is poised to be the micro-/nanofabrication tool of choice to manufacture multifunctional and complex micro-

/nanostructures, due to its ease of production, rapidly expanding pool of possible materials and substrates, as well as its competency in creating geometrically complicated 2D/3D micro-/nanostructures. We also recognize that the properties of self-customized photoresists can be further enhanced, and fabrication strategies can be more innovative for novel functional micro-/nanostructures. In fact, TPL as a 3D micro-/nanofabrication tool still faces multiple challenges in fabrication speed for large scale production, types and properties of photoresists, as well as structural stability and performance of TPL-fabricated micro-/nanostructures. Nevertheless, the advantages of TPL in 3D micro-/nanofabrication as showcased in this review give tremendous potential in providing breakthrough solutions for both fundamental research and product engineering in various fields. With this vision, we foresee the creation of novel two-photon processable photoresists and highly applicable 2D and 3D polymer/metallic microstructures that can be employed in conventional and emerging applications. The progress of TPL can potentially solve current technological challenges and invent novel structural materials that can accelerate production of prototypes for new products and expedite industrial problem-solving processes.

## AUTHOR INFORMATION

### **Corresponding Author**

\* Xing Yi Ling. E-mail: [xyling@ntu.edu.sg](mailto:xyling@ntu.edu.sg)

\* In Yee Phang. E-mail: [phangiy@imre.a-star.edu.sg](mailto:phangiy@imre.a-star.edu.sg)

### **Author Contributions**

The manuscript was written through contributions of all authors. All authors have given approval to the final version of the manuscript.

### **Note**

The authors declare no competing financial interest.

## ACKNOWLEDGMENT

X.Y.L. thanks the financial support from Singapore Ministry of Education, Tier 1 (RG11/18) and Tier 2 (MOE2016-T2-1-043) grants, and Max Planck Institute -Nanyang Technological University Joint Lab. C. S. L. Koh, G.C Phan-Quang, S. X. Leong thank the Nanyang President's Graduate Scholarships.

## REFERENCES

1. Xing, J.-F.; Zheng, M.-L.; Duan, X.-M., Two-photon polymerization microfabrication of hydrogels: an advanced 3D printing technology for tissue engineering and drug delivery. *Chem. Soc. Rev.* **2015**, *44* (15), 5031-5039.
2. Sugioka, K.; Cheng, Y., Femtosecond laser three-dimensional micro- and nanofabrication. *Appl. Phys. Rev.* **2014**, *1* (4), 041303.
3. Malinauskas, M.; Farsari, M.; Piskarskas, A.; Juodkasis, S., Ultrafast laser nanostructuring of photopolymers: A decade of advances. *Phys. Rep.* **2013**, *533* (1), 1-31.
4. Liu, X.; Gu, H.; Wang, M.; Du, X.; Gao, B.; Elbaz, A.; Sun, L.; Liao, J.; Xiao, P.; Gu, Z., 3D Printing of Bioinspired Liquid Superrepellent Structures. *Adv. Mater.* **2018**, *30* (22), 1800103.
5. Dong, Z.; Schumann, M. F.; Hokkanen, M. J.; Chang, B.; Welle, A.; Zhou, Q.; Ras, R. H. A.; Xu, Z.; Wegener, M.; Levkin, P. A., Superoleophobic Slippery Lubricant-Infused Surfaces: Combining Two Extremes in the Same Surface. *Adv. Mater.* **2018**, *30* (45), 1803890.
6. Lay, C. L.; Koh, C. S. L.; Wang, J.; Lee, Y. H.; Jiang, R.; Yang, Y.; Yang, Z.; Phang, I. Y.; Ling, X. Y., Aluminum nanostructures with strong visible-range SERS activity for versatile micropatterning of molecular security labels. *Nanoscale* **2018**, *10* (2), 575-581.
7. Mayer, F.; Richter, S.; Westhauser, J.; Blasco, E.; Barner-Kowollik, C.; Wegener, M., Multimaterial 3D laser microprinting using an integrated microfluidic system. *Sci. Adv.* **2019**, *5* (2), eaau9160.
8. Moroni, L.; Burdick, J. A.; Highley, C.; Lee, S. J.; Morimoto, Y.; Takeuchi, S.; Yoo, J. J., Biofabrication strategies for 3D in vitro models and regenerative medicine. *Nat. Rev. Mater.* **2018**, *3* (5), 21-37.
9. Murphy, S. V.; De Coppi, P.; Atala, A., Opportunities and challenges of translational 3D bioprinting. *Nat. Biomed. Eng.* **2019**.
10. Yin, X.; Fang, N.; Zhang, X.; Martini, I. B.; Schwartz, B. J., Near-field two-photon nanolithography using an apertureless optical probe. *Appl. Phys. Lett.* **2002**, *81* (19), 3663-3665.
11. Fourkas, J. T., Chapter 1.3 - Fundamentals of Two-Photon Fabrication. In *Three-Dimensional Microfabrication Using Two-photon Polymerization*, Baldacchini, T., Ed. William Andrew Publishing: Oxford, **2016**, pp 45-61.
12. Cui, Y.; Phang, I. Y.; Lee, Y. H.; Lee, M. R.; Zhang, Q.; Ling, X. Y., Multiplex plasmonic anti-counterfeiting security labels based on surface-enhanced Raman scattering. *Chem. Commun.* **2015**, *51* (25), 5363-5366.
13. Liu, Y.; Lee, Y. H.; Lee, M. R.; Yang, Y.; Ling, X. Y., Flexible Three-Dimensional Anticounterfeiting Plasmonic Security Labels: Utilizing Z-Axis-Dependent SERS Readouts to Encode Multilayered Molecular Information. *ACS Photonics* **2017**, *4* (10), 2529-2536.
14. Göring, G.; Dietrich, P.-I.; Blaicher, M.; Sharma, S.; Korvink, J. G.; Schimmel, T.; Koos, C.; Hölscher, H., Tailored probes for atomic force microscopy fabricated by two-photon polymerization. *Appl. Phys. Lett.* **2016**, *109* (6), 063101.

15. R  he, J., And There Was Light: Prospects for the Creation of Micro- and Nanostructures through Maskless Photolithography. *ACS Nano* **2017**, *11* (9), 8537-8541.
16. Delrot, P.; Loterie, D.; Psaltis, D.; Moser, C., Single-photon three-dimensional microfabrication through a multimode optical fiber. *Opt. Express* **2018**, *26* (2), 1766-1778.
17. Yoon, G.; Kim, I.; So, S.; Mun, J.; Kim, M.; Rho, J., Fabrication of three-dimensional suspended, interlayered and hierarchical nanostructures by accuracy-improved electron beam lithography overlay. *Sci. Rep.* **2017**, *7* (1), 6668.
18. Liu, N.; Guo, H.; Fu, L.; Kaiser, S.; Schweizer, H.; Giessen, H., Three-dimensional photonic metamaterials at optical frequencies. *Nat. Mater.* **2008**, *7* (1), 31-37.
19. Wu, S.; Serbin, J.; Gu, M., Two-photon polymerisation for three-dimensional micro-fabrication. *J. Photochem. Photobiol. A: Chem.* **2006**, *181* (1), 1-11.
20. Lu, D.-X.; Zhang, Y.-L.; Han, D.-D.; Wang, H.; Xia, H.; Chen, Q.-D.; Ding, H.; Sun, H.-B., Solvent-tunable PDMS microlens fabricated by femtosecond laser direct writing. *J. Mater. Chem. C* **2015**, *3* (8), 1751-1756.
21. Lv, C.; Sun, X.-C.; Xia, H.; Yu, Y.-H.; Wang, G.; Cao, X.-W.; Li, S.-X.; Wang, Y.-S.; Chen, Q.-D.; Yu, Y.-D.; Sun, H.-B., Humidity-responsive actuation of programmable hydrogel microstructures based on 3D printing. *Sensors Actuators B: Chem.* **2018**, *259*, 736-744.
22. Xiong, Z.; Zheng, M.-L.; Dong, X.-Z.; Chen, W.-Q.; Jin, F.; Zhao, Z.-S.; Duan, X.-M., Asymmetric microstructure of hydrogel: two-photon microfabrication and stimuli-responsive behavior. *Soft Matter* **2011**, *7* (21), 10353-10359.
23. Hippler, M.; Blasco, E.; Qu, J.; Tanaka, M.; Barner-Kowollik, C.; Wegener, M.; Bastmeyer, M., Controlling the shape of 3D microstructures by temperature and light. *Nat. Commun.* **2019**, *10* (1), 232.
24. Lee, M. R.; Phang, I. Y.; Cui, Y.; Lee, Y. H.; Ling, X. Y., Shape-Shifting 3D Protein Microstructures with Programmable Directionality via Quantitative Nanoscale Stiffness Modulation. *Small* **2015**, *11* (6), 740-748.
25. Lay, C. L.; Lee, M. R.; Lee, H. K.; Phang, I. Y.; Ling, X. Y., Transformative Two-Dimensional Array Configurations by Geometrical Shape-Shifting Protein Microstructures. *ACS Nano* **2015**, *9* (10), 9708-9717.
26. Huang, T.-Y.; Sakar, M. S.; Mao, A.; Petruska, A. J.; Qiu, F.; Chen, X.-B.; Kennedy, S.; Mooney, D.; Nelson, B. J., 3D Printed Microtransporters: Compound Micromachines for Spatiotemporally Controlled Delivery of Therapeutic Agents. *Adv. Mater.* **2015**, *27* (42), 6644-6650.
27. Ceylan, H.; Yasa, I. C.; Sitti, M., 3D Chemical Patterning of Micromaterials for Encoded Functionality. *Adv. Mater.* **2017**, *29* (9), 1605072.
28. Zhang, Q.; Lee, Y. H.; Phang, I. Y.; Lee, C. K.; Ling, X. Y., Hierarchical 3D SERS Substrates Fabricated by Integrating Photolithographic Microstructures and Self-Assembly of Silver Nanoparticles. *Small* **2014**, *10* (13), 2703-2711.
29. Tabrizi, S.; Cao, Y.; Lin, H.; Jia, B., Two-photon reduction: a cost-effective method for fabrication of functional metallic nanostructures. *Sci. China Phys. Mech.* **2017**, *60* (1674-7348), 034201.
30. Waller Erik, H.; von Freymann, G., From photoinduced electron transfer to 3D metal microstructures via direct laser writing. In *Nanophotonics*, **2018**; Vol. 7, p 1259.
31. Lee, M. R.; Lee, H. K.; Yang, Y.; Koh, C. S. L.; Lay, C. L.; Lee, Y. H.; Phang, I. Y.; Ling, X. Y., Direct Metal Writing and Precise Positioning of Gold Nanoparticles within Microfluidic Channels for SERS Sensing of Gaseous Analytes. *ACS Appl. Mater. Interfaces* **2017**, *9* (45), 39584-39593.
32. Xu, B.-B.; Zhang, R.; Liu, X.-Q.; Wang, H.; Zhang, Y.-L.; Jiang, H.-B.; Wang, L.; Ma, Z.-C.; Ku, J.-F.; Xiao, F.-S.; Sun, H.-B., On-chip fabrication of silver microflower arrays as a catalytic microreactor for allowing in situSERS monitoring. *Chem. Commun.* **2012**, *48* (11), 1680-1682.
33. Blasco, E.; M  ller, J.; M  ller, P.; Trouillet, V.; Sch  n, M.; Scherer, T.; Barner-Kowollik, C.; Wegener, M., Fabrication of Conductive 3D Gold-Containing Microstructures via Direct Laser Writing. *Adv. Mater.* **2016**, *28* (18), 3592-3595.
34. Xu, B.-B.; Zhang, D.-D.; Liu, X.-Q.; Wang, L.; Xu, W.-W.; Haraguchi, M.; Li, A.-W., Fabrication of microelectrodes based on precursor doped with metal seeds by femtosecond laser direct writing. *Opt. Lett.* **2014**, *39* (3), 434-437.
35. Zarzar, L. D.; Swartzentruber, B. S.; Harper, J. C.; Dunphy, D. R.; Brinker, C. J.; Aizenberg, J.; Kaehr, B., Multiphoton Lithography of Nanocrystalline Platinum and Palladium for Site-Specific Catalysis in 3D Microenvironments. *J. Am. Chem. Soc.* **2012**, *134* (9), 4007-4010.
36. Vyatskikh, A.; Delalande, S.; Kudo, A.; Zhang, X.; Portela, C. M.; Greer, J. R., Additive manufacturing of 3D nano-architected metals. *Nat. Commun.* **2018**, *9* (1), 593.

37. Jiang, L. J.; Maruo, S.; Osellame, R.; Xiong, W.; Campbell, J. H.; Lu, Y. F., Femtosecond laser direct writing in transparent materials based on nonlinear absorption. *MRS Bull.* **2016**, *41* (12), 975-983.
38. Gansel, J. K.; Thiel, M.; Rill, M. S.; Decker, M.; Bade, K.; Saile, V.; von Freymann, G.; Linden, S.; Wegener, M., Gold Helix Photonic Metamaterial as Broadband Circular Polarizer. *Science* **2009**, *325* (5947), 1513.
39. Liu, Y.; Lee, Y. H.; Zhang, Q.; Cui, Y.; Ling, X. Y., Plasmonic nanopillar arrays encoded with multiplex molecular information for anti-counterfeiting applications. *J. Mater. Chem. C* **2016**, *4* (19), 4312-4319.
40. Cui, Y.; Phang, I. Y.; Hegde, R. S.; Lee, Y. H.; Ling, X. Y., Plasmonic Silver Nanowire Structures for Two-Dimensional Multiple-Digit Molecular Data Storage Application. *ACS Photonics* **2014**, *1* (7), 631-637.
41. Mayer, F.; Richter, S.; Hübner, P.; Jabbour, T.; Wegener, M., 3D Fluorescence-Based Security Features by 3D Laser Lithography. *Adv. Mater. Technol.* **2017**, *2* (11), 1700212.
42. Liu, T. L.; Kim, C.-J. C., Turning a surface superrepellent even to completely wetting liquids. *Science* **2014**, *346* (6213), 1096.
43. Freire, M. G.; Carvalho, P. J.; Queimada, A. J.; Marrucho, I. M.; Coutinho, J. A. P., Surface Tension of Liquid Fluorocompounds. *J. Chem. Eng. Data* **2006**, *51* (5), 1820-1824.
44. Tottori, S.; Zhang, L.; Qiu, F.; Krawczyk, K. K.; Franco-Obregón, A.; Nelson, B. J., Magnetic Helical Micromachines: Fabrication, Controlled Swimming, and Cargo Transport. *Adv. Mater.* **2012**, *24* (6), 811-816.
45. Xia, H.; Wang, J.; Tian, Y.; Chen, Q.-D.; Du, X.-B.; Zhang, Y.-L.; He, Y.; Sun, H.-B., Ferrofluids for Fabrication of Remotely Controllable Micro-Nanomachines by Two-Photon Polymerization. *Adv. Mater.* **2010**, *22* (29), 3204-3207.
46. Power, M.; Thompson, A. J.; Anastasova, S.; Yang, G.-Z., A Monolithic Force-Sensitive 3D Microgripper Fabricated on the Tip of an Optical Fiber Using 2-Photon Polymerization. *Small* **2018**, *14* (16), 1703964.
47. Wei, S.; Liu, J.; Zhao, Y.; Zhang, T.; Zheng, M.; Jin, F.; Dong, X.; Xing, J.; Duan, X., Protein-Based 3D Microstructures with Controllable Morphology and pH-Responsive Properties. *ACS Appl. Mater. Interfaces* **2017**, *9* (48), 42247-42257.
48. Yi, H.; Seong, M.; Sun, K.; Hwang, I.; Lee, K.; Cha, C.; Kim, T.-i.; Jeong, H. E., Wet-Responsive, Reconfigurable, and Biocompatible Hydrogel Adhesive Films for Transfer Printing of Nanomembranes. *Adv. Funct. Mater.* **2018**, *28* (18), 1706498.
49. Yin, M.-J.; Yao, M.; Gao, S.; Zhang, A. P.; Tam, H.-Y.; Wai, P.-K. A., Rapid 3D Patterning of Poly(acrylic acid) Ionic Hydrogel for Miniature pH Sensors. *Adv. Mater.* **2016**, *28* (7), 1394-1399.
50. Lay, C. L.; Lee, Y. H.; Lee, M. R.; Phang, I. Y.; Ling, X. Y., Formulating an Ideal Protein Photoresist for Fabricating Dynamic Microstructures with High Aspect Ratios and Uniform Responsiveness. *ACS Appl. Mater. Interfaces* **2016**, *8* (12), 8145-8153.
51. Spivey, E. C.; Ritschdorff, E. T.; Connell, J. L.; McLennon, C. A.; Schmidt, C. E.; Shear, J. B., Multiphoton Lithography of Unconstrained Three-Dimensional Protein Microstructures. *Adv. Funct. Mater.* **2013**, *23* (3), 333-339.
52. Su, S.; Pelton, R., Bovine Serum Albumin (BSA) as an adhesive for wet cellulose. *Cellulose* **2006**, *13* (5), 537-545.
53. Ovsianikov, A.; Mühleder, S.; Torgersen, J.; Li, Z.; Qin, X.-H.; Van Vlierberghe, S.; Dubruel, P.; Holnthoner, W.; Redl, H.; Liska, R.; Stampfl, J., Laser Photofabrication of Cell-Containing Hydrogel Constructs. *Langmuir* **2014**, *30* (13), 3787-3794.
54. Huang, X.; Wang, X.; Zhao, Y., Study on a series of water-soluble photoinitiators for fabrication of 3D hydrogels by two-photon polymerization. *Dyes Pigm.* **2017**, *141*, 413-419.
55. Mu, J.; Hou, C.; Wang, H.; Li, Y.; Zhang, Q.; Zhu, M., Origami-inspired active graphene-based paper for programmable instant self-folding walking devices. *Sci. Adv.* **2015**, *1* (10), e1500533.
56. Liu, Y.; Shaw, B.; Dickey, M. D.; Genzer, J., Sequential self-folding of polymer sheets. *Sci. Adv.* **2017**, *3* (3), e1602417.
57. Nawroth, J. C.; Lee, H.; Feinberg, A. W.; Ripplinger, C. M.; McCain, M. L.; Grosberg, A.; Dabiri, J. O.; Parker, K. K., A tissue-engineered jellyfish with biomimetic propulsion. *Nat. Biotechnol.* **2012**, *30* (8), 792-797.
58. Nayak, L.; Mohanty, S.; Nayak, S. K.; Ramadoss, A., A review on inkjet printing of nanoparticle inks for flexible electronics. *J. Mater. Chem. C* **2019**, *7* (29), 8771-8795.
59. Tanaka, T.; Ishikawa, A.; Kawata, S., Two-photon-induced reduction of metal ions for fabricating three-dimensional electrically conductive metallic microstructure. *Appl. Phys. Lett.* **2006**, *88* (8), 081107.
60. Kang, S.; Vora, K.; Mazur, E., One-step direct-laser metal writing of sub-100 nm 3D silver nanostructures in a gelatin matrix. *Nanotechnology* **2015**, *26* (12), 121001.

61. Vanýsek, P., Electrochemical Series. In *CRC Handbook of Chemistry and Physics*, 91 ed.; Haynes, W. M., Ed. Taylor & Francis: **2010**.
62. Maruo, S.; Saeki, T., Femtosecond laser direct writing of metallic microstructures by photoreduction of silver nitrate in a polymer matrix. *Opt. Express* **2008**, *16* (2), 1174-1179.
63. Focsan, M.; Craciun, A. M.; Astilean, S.; Baldeck, P. L., Two-photon fabrication of three-dimensional silver microstructures in microfluidic channels for volumetric surface-enhanced Raman scattering detection. *Opt. Mater. Express* **2016**, *6* (5), 1587-1593.
64. Tabrizi, S.; Cao, Y.; Cumming, B. P.; Jia, B.; Gu, M., Functional Optical Plasmonic Resonators Fabricated via Highly Photosensitive Direct Laser Reduction. *Adv. Opt. Mater.* **2016**, *4* (4), 529-533.
65. Izquierdo-Lorenzo, I.; Jradi, S.; Adam, P.-M., Direct laser writing of random Au nanoparticle three-dimensional structures for highly reproducible micro-SERS measurements. *RSC Adv.* **2014**, *4* (8), 4128-4133.
66. Cao, Y.; Gu, M.,  $\lambda/26$  silver nanodots fabricated by direct laser writing through highly sensitive two-photon photoreduction. *Appl. Phys. Lett.* **2013**, *103* (21), 213104.
67. Ishikawa, A.; Tanaka, T.; Kawata, S., Improvement in the reduction of silver ions in aqueous solution using two-photon sensitive dye. *Appl. Phys. Lett.* **2006**, *89* (11), 113102.
68. Shukla, S.; Vidal, X.; Furlani, E. P.; Swihart, M. T.; Kim, K.-T.; Yoon, Y.-K.; Urbas, A.; Prasad, P. N., Subwavelength Direct Laser Patterning of Conductive Gold Nanostructures by Simultaneous Photopolymerization and Photoreduction. *ACS Nano* **2011**, *5* (3), 1947-1957.
69. Cao, Y.-Y.; Takeyasu, N.; Tanaka, T.; Duan, X.-M.; Kawata, S., 3D Metallic Nanostructure Fabrication by Surfactant-Assisted Multiphoton-Induced Reduction. *Small* **2009**, *5* (10), 1144-1148.
70. He, G.-C.; Zheng, M.-L.; Dong, X.-Z.; Jin, F.; Liu, J.; Duan, X.-M.; Zhao, Z.-S., The Conductive Silver Nanowires Fabricated by Two-beam Laser Direct Writing on the Flexible Sheet. *Sci. Rep.* **2017**, *7* (1), 41757.
71. Tan, E. K. W.; Rughoobur, G.; Rubio-Lara, J.; Tiwale, N.; Xiao, Z.; Davidson, C. A. B.; Lowe, C. R.; Occhipinti, L. G., Nanofabrication of Conductive Metallic Structures on Elastomeric Materials. *Sci. Rep.* **2018**, *8* (1), 6607.
72. Lu, W.-E.; Zhang, Y.-L.; Zheng, M.-L.; Jia, Y.-P.; Liu, J.; Dong, X.-Z.; Zhao, Z.-S.; Li, C.-B.; Xia, Y.; Ye, T.-C.; Duan, X.-M., Femtosecond direct laser writing of gold nanostructures by ionic liquid assisted multiphoton photoreduction. *Opt. Mater. Express* **2013**, *3* (10), 1660-1673.
73. Abgrall, P.; Gué, A. M., Lab-on-chip technologies: making a microfluidic network and coupling it into a complete microsystem—a review. *J. Micromech. Microeng.* **2007**, *17* (5), R15-R49.
74. Dicken, M. J.; Aydin, K.; Pryce, I. M.; Sweatlock, L. A.; Boyd, E. M.; Walavalkar, S.; Ma, J.; Atwater, H. A., Frequency tunable near-infrared metamaterials based on VO<sub>2</sub> phase transition. *Opt. Express* **2009**, *17* (20), 18330-18339.
75. Yue, W.; Wang, Z.; Whittaker, J.; Schedin, F.; Wu, Z.; Han, J., Resonance control of mid-infrared metamaterials using arrays of split-ring resonator pairs. *Nanotechnology* **2016**, *27* (5), 055303.
76. Hu, Q.; Sun, X.-Z.; Parmenter, C. D. J.; Fay, M. W.; Smith, E. F.; Rance, G. A.; He, Y.; Zhang, F.; Liu, Y.; Irvine, D.; Tuck, C.; Hague, R.; Wildman, R., Additive manufacture of complex 3D Au-containing nanocomposites by simultaneous two-photon polymerisation and photoreduction. *Sci. Rep.* **2017**, *7* (1), 17150-17150.
77. Fogel, O.; Kotler, Z.; Zalevsky, Z., Towards 3D digital printing of micro-electromechanical systems. *NIP & Digital Fabrication Conference* **2018**, *2018* (1), 186-188.
78. Zhang, D.; Wei, B., *Advanced Mechatronics and MEMS Devices II*. Springer International Publishing: **2016**.
79. Burek, M. J.; Greer, J. R., Fabrication and Microstructure Control of Nanoscale Mechanical Testing Specimens via Electron Beam Lithography and Electroplating. *Nano Lett.* **2010**, *10* (1), 69-76.
80. Daryadel, S.; Behroozfar, A.; Morsali, S. R.; Moreno, S.; Baniasadi, M.; Bykova, J.; Bernal, R. A.; Minary-Jolandan, M., Localized Pulsed Electrodeposition Process for Three-Dimensional Printing of Nanotwinned Metallic Nanostructures. *Nano Lett.* **2018**, *18* (1), 208-214.
81. Radke, A.; Gissibl, T.; Klotzbücher, T.; Braun, P. V.; Giessen, H., Three-Dimensional Bichiral Plasmonic Crystals Fabricated by Direct Laser Writing and Electroless Silver Plating. *Adv. Mater.* **2011**, *23* (27), 3018-3021.
82. Zeeshan, M. A.; Grisch, R.; Pellicer, E.; Sivaraman, K. M.; Peyer, K. E.; Sort, J.; Özkale, B.; Sakar, M. S.; Nelson, B. J.; Pané, S., Hybrid Helical Magnetic Microrobots Obtained by 3D Template-Assisted Electrodeposition. *Small* **2014**, *10* (7), 1284-1288.
83. Machida, M.; Niidome, T.; Onoe, H.; Heisterkamp, A.; Terakawa, M., Spatially-targeted laser fabrication of multi-metal microstructures inside a hydrogel. *Opt. Express* **2019**, *27* (10), 14657-14666.

84. Cui, Y.; Hegde, R. S.; Phang, I. Y.; Lee, H. K.; Ling, X. Y., Encoding molecular information in plasmonic nanostructures for anti-counterfeiting applications. *Nanoscale* **2014**, *6* (1), 282-288.

**Table 1.** Types of microstructures fabricated from commercial photoresists and their applications.

Commercial photoresists					
Photoresist	Structures	Subsidiary approach/Additives	Status	Applications	Ref.
Acrylate-based IP-L 780	Nanowires	Thermal evaporation of silver with 150 nm thick, 2-naphthalenethiol and 4-MBT as probe molecule:	Stationary	2D anti-counterfeiting label	84
Acrylate-based IP-L 780	Nanowires and nanodots	Thermal evaporation of 100 nm-thick aluminum film. Naphthalene and triethyl(phenyl)silane as probe molecules	Stationary	Two-tier security labels with quick-response code and ciphertxts	6
Acrylate-based IP-L 780	Double-layered nanowires	Thermal evaporation of silver with 150 nm thick, rhodamine B isothiocyanate and 4-MBT as probe molecules	Stationary	Multiplex security labels	12
Acrylate-based IP-L 780	Nanodots	Thermal evaporation of silver with 100 nm thick	Stationary	Multiplex security labels	39
Acrylate-based IP-L 780	Micron-sized pyramids	Langmuir-Blodgett assisted self-assembly of 100-nm silver nanocubes	Stationary	3D micro-barcode	28
Acrylate-based IP-Dip	Candlestick microstructures	Thermal evaporation of silver with 100 nm thick	Stationary	3D micro-barcode	13
Pentaerythritol triacrylate with Irgacure 819	3D non-labeled cross-grid and quantum dots	CdSSe/ZnS core-shell quantum dots embedded photoresists	Stationary	3D fluorescent security features	41
Acrylate-based IP-S	Triply re-entrant microstructures	Not applicable	Stationary	Superomniphobic surfaces	4
Acrylate-based IP-Dip	Doubly re-entrant structures with lubricant-infused porous surfaces	Surface was modified with perfluorooctyl-trichlorosilane was infused with lubricant oil	Stationary	Superomniphobic surfaces	5
Epoxy-based SU-8 and acrylate-based IP-L 780	Helical microstructures with holder	Deposition of nickel and titanium bilayer via e-beam evaporation	Mobile	Magnetic-driven micromanipulation of biological samples	44
Epoxy-based SU-8	Microtransporters with cylinder and screw-like piston	Outer surface of cylinder was functionalized with polyethylene glycol. Plunger was coated with nickel and titanium bilayer	Mobile	Microtransporter for targeted controlled drug and cell delivery	26.
Iron oxide-containing acrylates	Microturbines	Not applicable	Mobile	Micromixer and micro-generator	45
Poly(ethylene glycol) diacrylate and Irgacure 369	Bullet-like microstructures with inner cavity	Selective patterning inner cavity with carboxylic acid moieties	Mobile	Hydrogen peroxide-driven swimmer as diagnostic device and cargo carrier	27

Acrylate-based IP-Dip	Microgrippers with 3 fingers	Not applicable	Mobile	Microgrippers for cellular manipulation and surgery	46
--------------------------	---------------------------------	----------------	--------	--	----

**Table 2.** Types of stimuli-responsive microstructures fabricated from customizable hydrogel/organogel formulations and their applications.

Hydrogel/organogel photoresists				
Photoresist	Structures	Stimulus / Type of swelling	Applications	Ref.
Acrylates, 2,4,6-trimethylbenzoyldiphenyl phosphine oxide and phenylbis (2,4,6-trimethylbenzoyl) phosphine oxide	Stomata-like hydrogel microstructures, binary codes micropillar, joint-like cantilever microstructure	Water / Uniform swelling	Moisture sensors, security labels and actuators	21
PDMS with thioxanthen-9-one	Aspheric hyperboloid microstructures	Solvent / Uniform swelling	Microlens	20
Bovine serum albumin with rose bengal	2.5D panda-like structures, grid/sieve-shaped microstructures	pH / Uniform swelling	pH sensors, microsieves	47
Bovine serum albumin with rose bengal	Chiral microstructures and microtrap with bimetallic-based design	pH / Non-uniform swelling	Actuators	24
Bovine serum albumin with rose bengal	Geometrical shape-shifting microstructures with sandwich-based design	pH / Non-uniform swelling	Microfluidics, cell micropatterning	25
Poly(acrylamide-2-acrylamido-2-methylpropane sulfonic acid sodium)	Pillars with bimetallic-based design	Salt / Non-uniform swelling	Actuators	22
<i>N</i> -isopropylacrylamide and lithium phenyl(2,4,6-trimethylbenzoyl)phosphinate in ethylene glycol	3D hetero-microstructures with bimetallic-based design	Temperature / Non-uniform swelling	Actuators	23

**Table 3.** Types of microstructures fabricated from various metal-salt based photoresists formulations and their applications.

Metal-salt based photoresists					
Types of metal salt	Subsidiary approach/Additives	Structures	Status	Applications	Ref.
Gold (III) chloride trihydrate	Epoxy-based SU-8 photoresist as supporting matrix	Lines, nanoflower, nanoblocks and fishnet structures	2D metal structures in polymer on glass	Split ring resonator and SERS substrates	68
Gold (III) chloride trihydrate	Trimethylolpropane ethoxylate triacrylate, acrylic acid, 3-(trimethoxysilyl) propyl methacrylate	Lines	Polymer coated metal structures on glass	Connectors for electronic circuit	33
Gold (III) chloride trihydrate	Surfactant CTAB	Nanodots and 2.5D woodpile structures	Metallic structures on glass	SERS substrates	65
Gold (III) chloride trihydrate	Various ionic liquids as capping agents	2D patterns and 2.5D U-shaped structures	Metallic structures on glass	Split-ring resonators (SRRs)	72
Silver nitrate	Gelatine	Nanodots	A ten-layered metal dots inside gelatine on glass	Tuneable optical devices	60
Diamine silver ions	Surfactant n-decanoysarcosine sodium	Lines, pillars and 3D pyramids	Metallic structures on glass	Not mentioned	69
Silver nitrate	Poly(vinylpyrrolidone)	Lines	Metallic structures on glass and within glass micro-tubes	SERS substrates	31
Silver nitrate	(2-hydroxy-4'-(2-hydroxyethoxy)-2-methylpropiophenone (HHMP) was photosensitizer and (n-decanoysarcosine sodium (NDSS) as surfactant	C-shaped lines	Metallic structures on glass	Split-ring resonators (SRRs)	64
Ammonium tetrachloroplatinate (II) salt	Ammonium trisoxalatoferrate (III) trihydrate as photosensitizer	2D patterns	Metallic structures on glass	Catalysts	35
Nickel 2-methoxyethoxide and acrylic acid	Pentaerythritol triacrylate and 7-diethylamino-3-thenoylcoumarin. Pyrolysis to remove acrylate polymer	Tetrakaidekahedron unit cell, 3D nickel octet nanolattices	3D metal structures with/without polymer on glass	Miniature mechanical devices, 3D microbattery electrodes	36

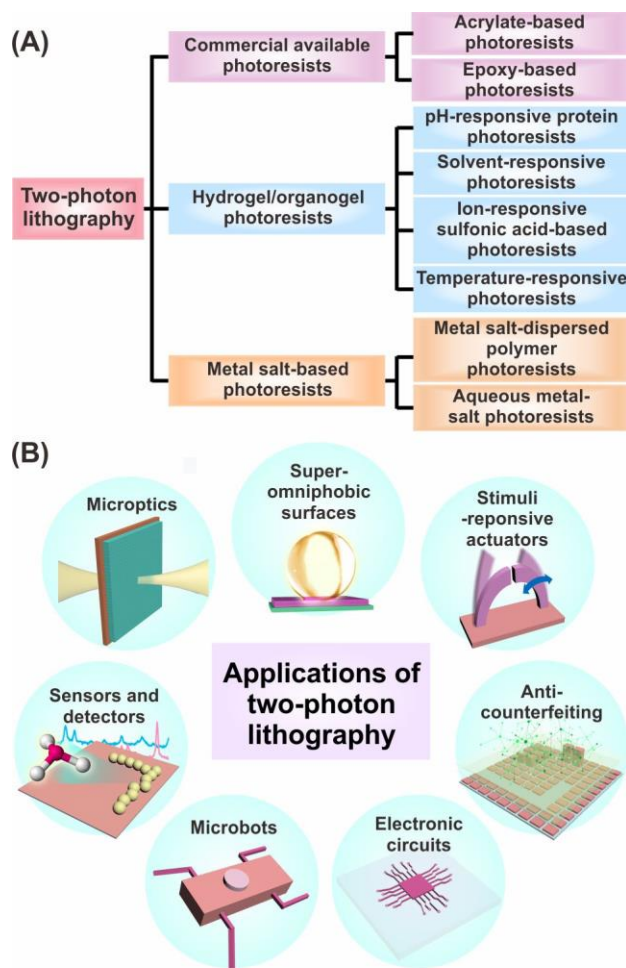


**Figure 1.** Overview of two-photon lithography photoresists and applications. (A) Classification of the types of photoresist used in two-photon lithography. (B) Applications of the microstructures fabricated via two-photon lithography.

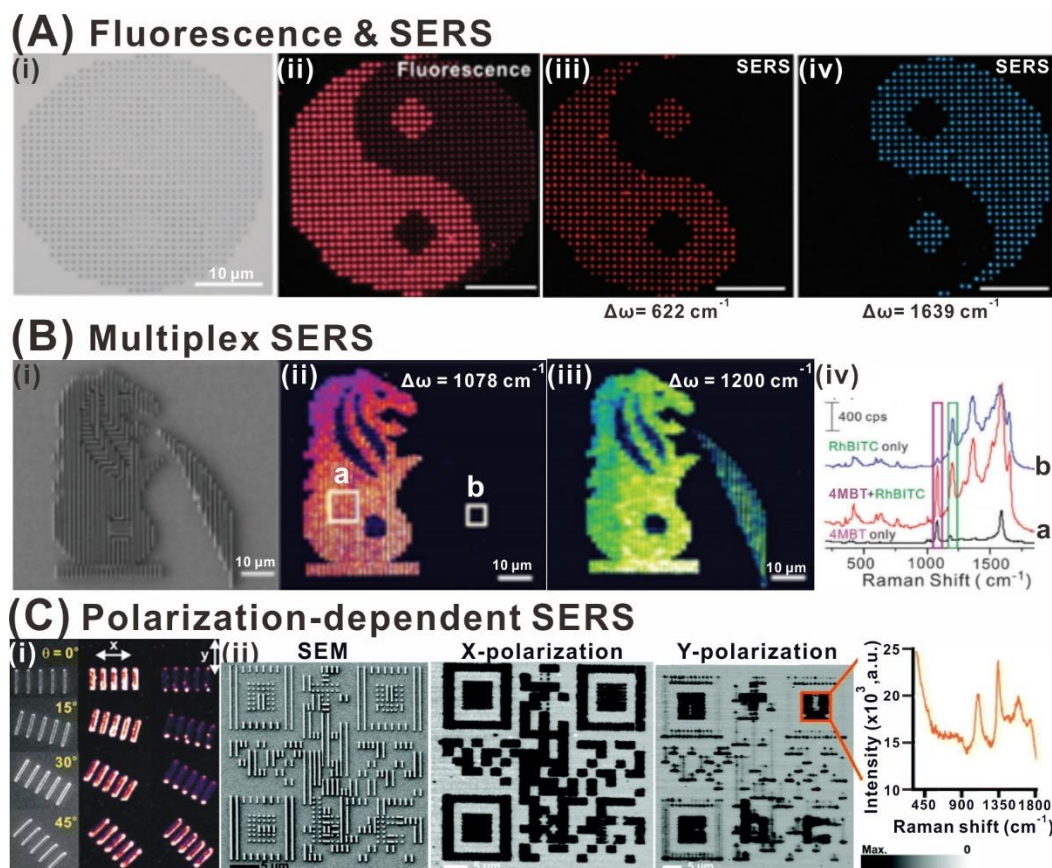


**Figure 2.** 2D microstructure pattern combined with SERS readout as security anti-counterfeiting labels. (A) Security label consisting of rhodamine-6G (R6G)- and eosin Y (EY)-encapsulated nanopillars. (i) Bright-field microscopic and (ii) the covert pattern decoded via fluorescence spectroscopy. (iii, iv) SERS hyperspectral images revealing the complementary patterns when specific wavenumbers of R6G and EY SERS fingerprints are selected respectively. Reproduced from ref. 39 with permission from The Royal Society of Chemistry. (B) (i) SEM image and (ii, iii) different 2D SERS hyperspectral images of multiplex SERS security label showing a Merlion without and with a water stream when selecting different characteristic wavenumber. Reproduced from ref. 12 with permission from The Royal Society of Chemistry. (C) (i) SEM and corresponding x- and y-polarized 2D SERS images of Ag nanowires with SERS intensity depends on orientation angles. Adapted with permission from ref. 40. Copyright 2014 American Chemical Society. (ii)

Two-tier security label that reveals a quick-response (QR) code or ciphertexts when x- and y-polarization light are used respectively. Molecular fingerprint of the embedded naphthalene serves as additional covert information. Reproduced from ref. 6 with permission from The Royal Society of Chemistry.

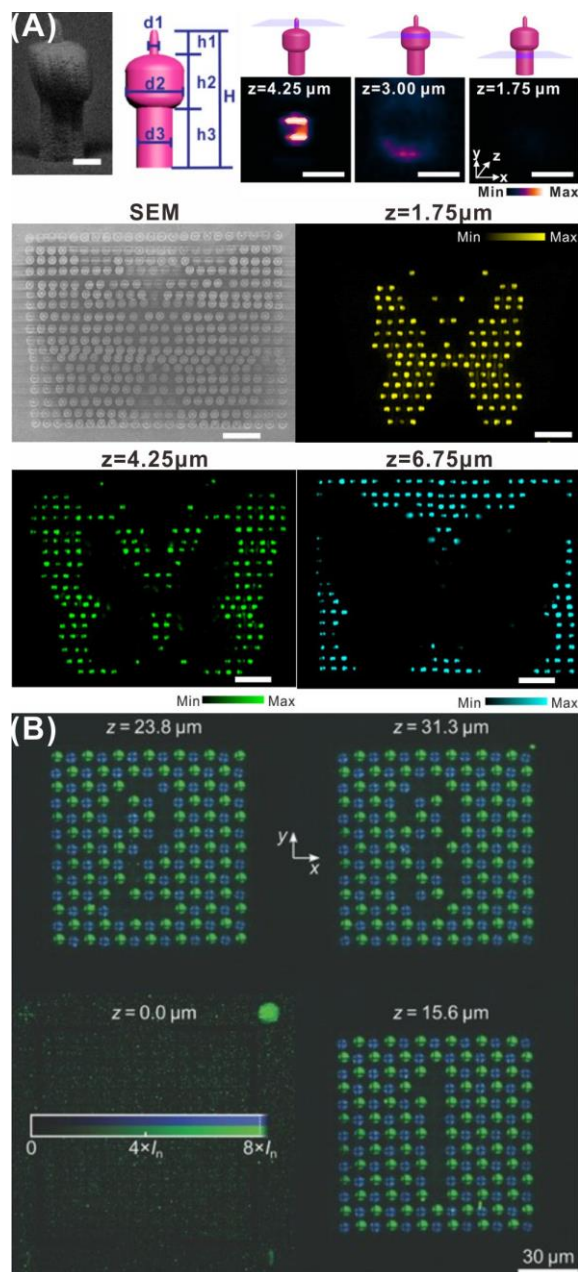


**Figure 3.** 3D microstructure pattern combined with SERS readout as security anti-counterfeiting labels. (A) SEM and Schematic image of a polymeric 3D candlestick and its  $z$ -dependent SERS readouts. The resultant array forms a three-layered 3D SERS security label that reveals three different butterfly patterns at different  $z$ -distance. Adapted with permission from ref. 13. Copyright (2017) American Chemical Society. (B) 3D tooth-like crossed-grid embedded with quantum dots

reveals highly z-dependent numerical patterns via fluorescence imaging. Reproduced with permission from ref. 41. Copyright 2017 John Wiley & Sons, Ltd.

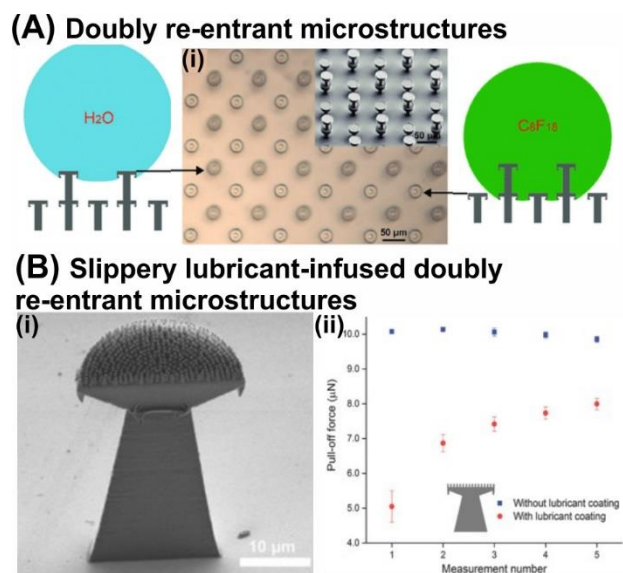


**Figure 4.** Superomniphobic doubly re-entrant microstructures fabricated via two-photon lithography. (A)(i) Optical and SEM image (inset) of an array of double-layered doubly re-entrant microstructures which can repel both water and n-perfluorooctane. Reproduced with permission from ref. 4. Copyright 2018 John Wiley & Sons, Ltd. (B)(i) Cross-sectional SEM image of a doubly re-entrant micropillar with a nanorough top. (ii) Efficiency and repeatability on surface repellency of the doubly re-entrant micropillars via microscopic droplet pull-off force (equivalent to surface adhesion force) measurements on individual micropillars with (red circles) and without (blue squares) lubricant coating. Reproduced with permission from ref. 5. Copyright 2018 John Wiley & Sons, Ltd.

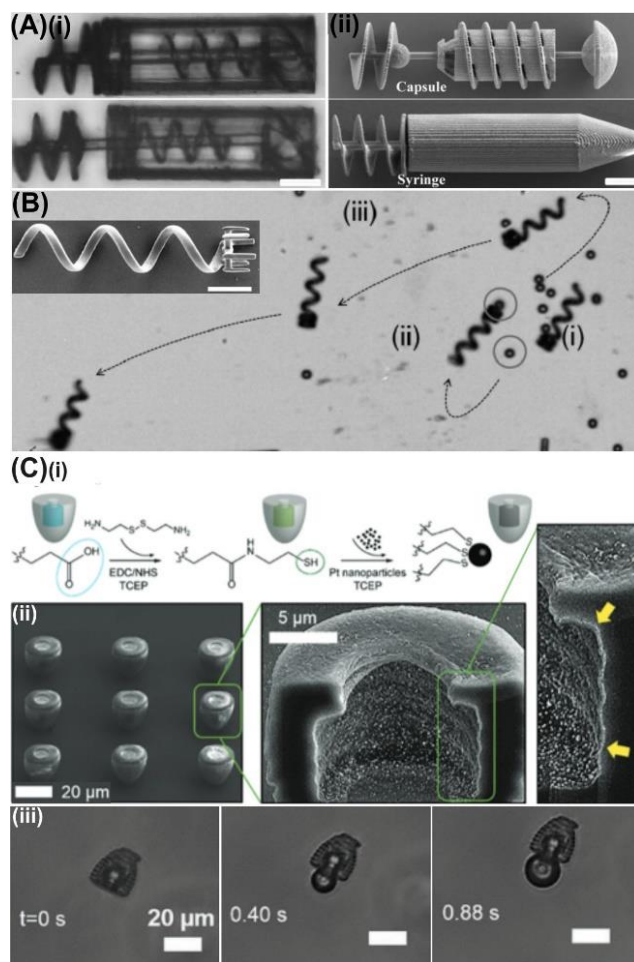


**Figure 5.** Fabrication and application of microrobots using TPP. (A)(i and ii) TEM and SEM image of a compound microtransporter with multiple mechanical components, respectively. Reproduced with permission from ref. 26. Copyright 2015, John Wiley & Sons Inc. (B) Time-lapse image of the transportation of a microparticle from (i) to (v) by a helical microholder (inset) that is manipulated via an external magnetic field. Adapted with permission from ref. 44. Copyright 2012, John Wiley & Sons Inc. (C)(i) Schematic representation on site-selective formation of sulfhydryl groups ( $-SH$ ) of the microswimmer for targeted platinum nanoparticles attachment at the inner cavity (shown in ii). This enables compartmentalized degradation of hydrogen peroxide by platinum (Pt) which results in the self-propulsion of the microswimmer. (iii)

Digital images of a microswimmer within a single bubble growth cycle in 2% hydrogen peroxide.

Adapted with permission from ref. 27. Copyright 2016, John Wiley & Sons Inc.

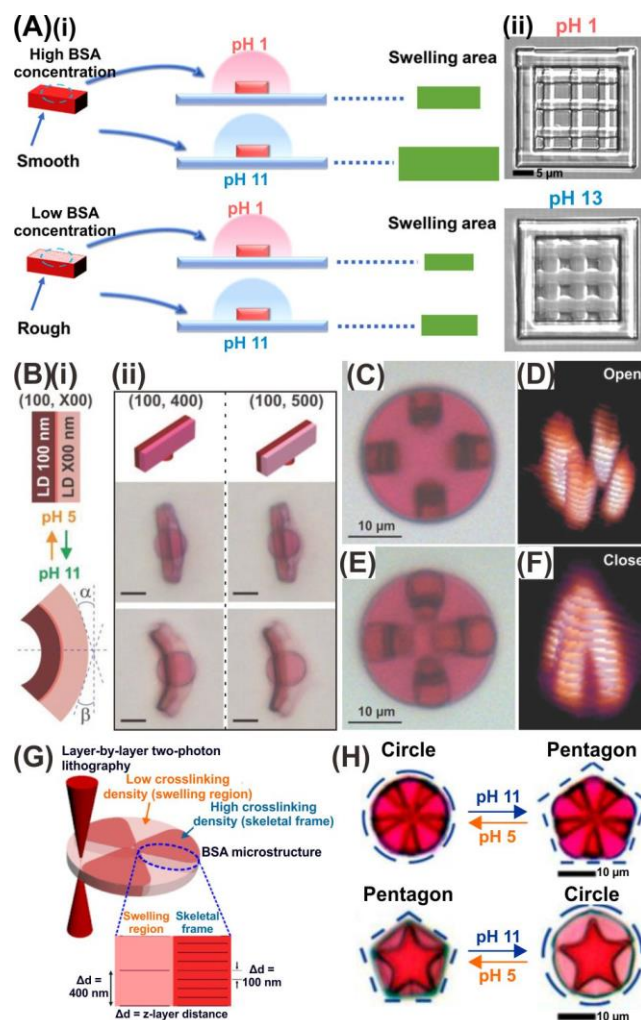
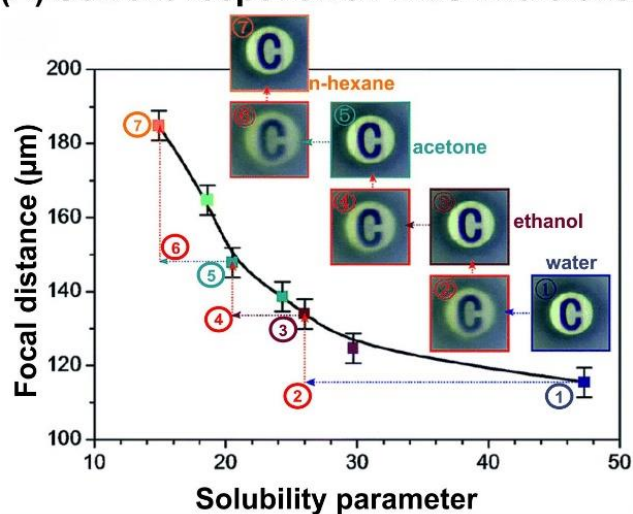


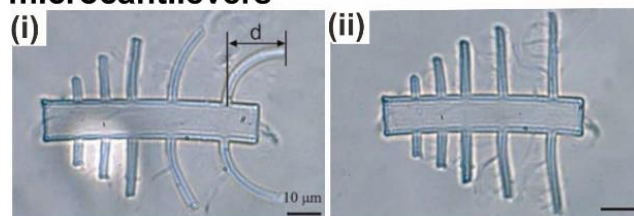
**Figure 6.** pH-responsive dynamic protein microstructures created from TPP. (A) (i) Schematic illustration of swelling state of microstructures fabricated using different BSA concentrations via TPP. (ii) Bright field images of BSA microsieves at different pH. Reprinted (adapted) with permission from ref. 47. Copyright 2017 American Chemical Society. (B) To achieve anisotropic hydrogel swelling, crosslinking density is maneuvered by varying the z-layer distance ( $\Delta d$ ) during the layer-by-layer TPP. (B) (i, ii) Schematic and digital images of “bimetallic” BSA strips made of different crosslinking densities. The “bimetallic” strip bends in pH 11 solution because the BSA region that has lower crosslinking density expands to a larger extent. (C, E) Optical image and (D, F) 3D Raman imaging of a dynamic 3D Venus flytrap structure which “opens” and “closes” at pH

5 and 11, respectively. Adapted with permission from ref. 24. Copyright 2014, John Wiley & Sons Inc. (G) Schematic of dynamic geometrical shape-shifting BSA microstructure fabricated via the spatial modulation of the z-layer distance using two-photon lithography to alter the crosslinking density within a structure. The resultant BSA microstructures can shapeshift from (H) Circle-to-pentagon and pentagon-to-circle under different pH. Adapted with permission from ref. 25. Copyright 2015 American Chemical Society.

### (A) Solvent-responsive PDMS microlens



### (B) Ion-responsive sulfonic acid-based microcantilevers



### (C) Temperature-responsive PNIPAAm hetero-structures



**Figure 7.** Stimuli-responsive polymer microstructures. (A) Uniform swelling of PDMS micro-lens and the change in focal length of the lens that is dependent on the stimuli solvents of different solubility parameters. Reproduced from ref. 20 with permission from The Royal Society of Chemistry. The insets are the images viewed through the PDMS micro-lens after immersion in different solvents at the respective focal distance. (B) Bending behavior of microcantilevers made of 2-acrylamido-2-methylpropane sulfonic acid sodium (AMPS) with acrylamide (AAm) (poly(AMPS-AAm)) (i) in water and (ii) in 1 M NaCl. Reproduced from ref. 22 with permission from The Royal Society of Chemistry. (C) Temperature-dependent bending behavior of 3D hetero-

microstructures made of poly(N-isopropylacrylamide) (PNIPAAm) in water at (i) 20 °C and (ii) 45 °C. Reproduced from ref. 23. Copyright 2019 Nature Publishing Group.

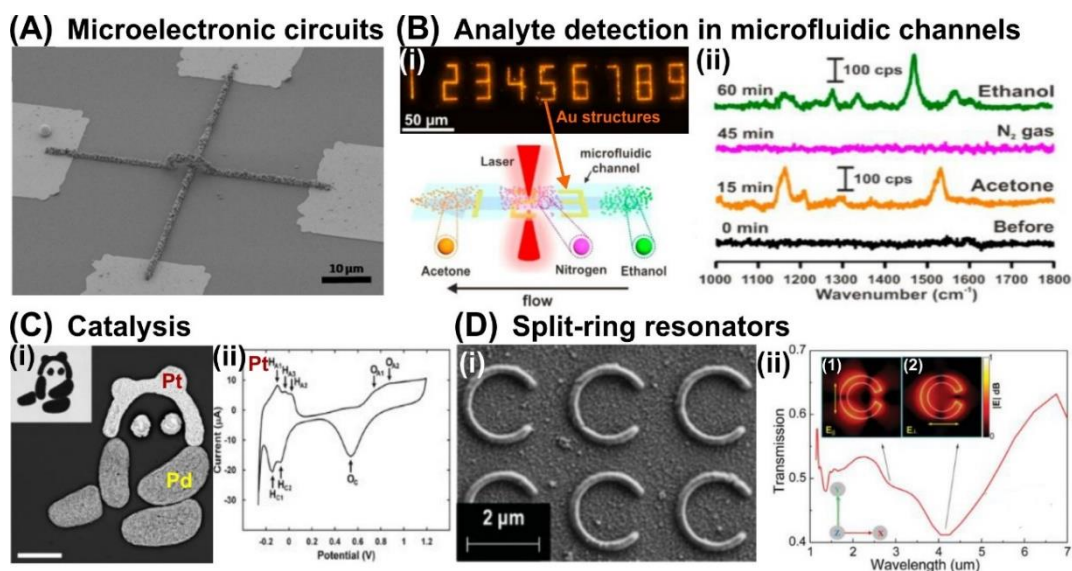


**Figure 8.** DMW of 2D metallic microstructures. (A) Particulate-like Au wires connecting the 4 electrodes employed for the four-point conductivity measurements. Reproduced with permission from ref. 33. Copyright 2015, John Wiley & Sons Inc. (B) (i) SERS hyperspectral image of the gold (Au) structures written in a microfluidic tube. (ii) SERS spectra demonstrating the sequential detection of gaseous acetone and ethanol after flushing with nitrogen gas. Adapted with permission from ref. 31. Copyright 2017 American Chemical Society. (C) (i) Graphical pattern of a panda with site-selective DMW of platinum (Pt) and palladium (Pd) demonstrating the precision of TPL on multi-materials patterning at pre-designated areas. (ii) Cyclic voltammetry of DMW-Pt working electrode in 1.0 M  $\text{H}_2\text{SO}_4$  to characterize its electrocatalytic response. Adapted with permission from ref. 35. Copyright 2012 American Chemical Society. (D) (i) An array of c-shaped Ag split-ring resonators (SRRs) with (ii) transmission spectrum showing the two Mie-type resonances when the polarization is (1) parallel and (2) perpendicular to the gap. Reproduced with permission from ref. 64. Copyright 2015, John Wiley & Sons Inc.

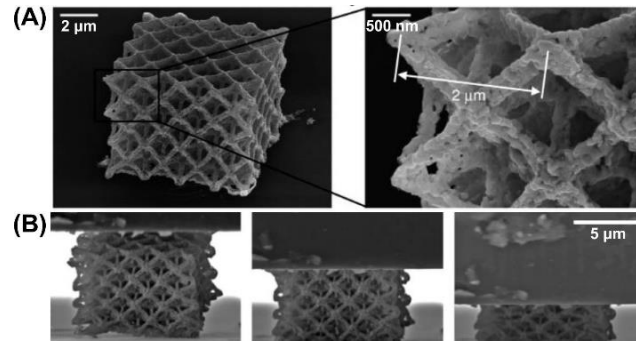


**Figure 9.** DMW of 3D metallic metamaterials. (A) A representative nickel (Ni) nanolattice after pyrolysis and its magnified image. (B) In situ uniaxial compression of the 3D printed Ni octet nanolattices before compression to its elastic regime, and eventually reaching layer-by-layer collapse (left to right, respectively). Reproduced from ref. 36. Copyright 2018 Nature Publishing Group.

**Optimum photoresist formulation in 3D nanofabrication via two-photon polymerization and reduction** is crucial to generate functional micro-/nanostructures for emerging applications. Our review highlights emerging applications of commercial photoresists and gel-/metal salt-based photoresists, as well as addresses the challenges encountered in formulating processable photoresists for two-photon lithography.

**KEYWORDS:** Two-photon lithography, two-photon polymerization, two-photon reduction, direct metal writing, 3D nanofabrication, hydrogel/organogel photoresists, metal salt-based photoresists

*Chee Leng Lay<sup>†‡</sup>, Charlynn Sher Lin Koh<sup>†</sup>, Yih Hong Lee<sup>†</sup>, Gia Chuong Phan-Quang<sup>†</sup>, Howard Yi Fan Sim<sup>†</sup>, Shi Xuan Leong<sup>†</sup>, Xuemei Han<sup>†</sup>, In Yee Phang<sup>\*†</sup> and Xing Yi Ling<sup>\*†</sup>*

## **Two-photon-assisted Polymerization and Reduction: Emerging Formulations and Applications**

